Journal of Experimental Botany, Vol. 70, No. 20 pp. 5943–5958, 2019
doi:10.1093/jxb/erz348 Advance Access Publication July 31, 2019
This paper is available online free of all access charges (see https://academic.oup.com/jxb/pages/openaccess for further details)

RESEARCH PAPER

A MIF-like effector suppresses plant immunity and facilitates nematode parasitism by interacting with plant annexins

Jianlong Zhao[1], Lijuan Li[1], Qian Liu[1], Pei Liu[1], Shuang Li[1], Dan Yang[1], Yongpan Chen[1], Sophie Pagnotta[2], Bruno Favery[3], Pierre Abad[3] and Heng Jian[1,*]

[1] Department of Plant Pathology and Key Laboratory of Pest Monitoring and Green Management of the Ministry of Agriculture, China Agricultural University, Beijing 100193, China
[2] Centre Commun de Microscopie Appliquée (CCMA), Université de Nice Sophia Antipolis, Nice, France
[3] Université Côte d'Azur, INRA, CNRS, ISA, France

* Correspondence: hengjian@cau.edu.cn

Received 15 November 2018; Editorial decision 16 July 2019; Accepted 22 July 2019

Editor: Miriam Gifford, University of Warwick, UK

Abstract

Plant-parasitic nematodes secrete numerous effectors to facilitate parasitism, but detailed functions of nematode effectors and their plant targets remain largely unknown. Here, we characterized four macrophage migration inhibitory factors (MIFs) in *Meloidogyne incognita* resembling the MIFs secreted by human and animal parasites. Transcriptional data showed *MiMIFs* are up-regulated in parasitism. Immunolocalization provided evidence that MiMIF proteins are secreted from the nematode hypodermis to the parasite surface, detected in plant tissues and giant cells. *In planta MiMIFs* RNA interference in Arabidopsis decreased infection and nematode reproduction. Transient expression of MiMIF-2 could suppress Bax- and RBP1/Gpa2-induced cell death. *MiMIF-2* ectopic expression led to higher levels of Arabidopsis susceptibility, suppressed immune responses triggered by flg22, and impaired $[Ca^{2+}]_{cyt}$ influx induced by H_2O_2. The immunoprecipitation of MiMIF-2-interacting proteins, followed by co-immunoprecipitation and bimolecular fluorescence complementation validations, revealed specific interactions between MiMIF-2 and two Arabidopsis annexins, AnnAt1 and AnnAt4, involved in the transport of calcium ions, stress responses, and signal transduction. Suppression of expression or overexpression of these annexins modified nematode infection. Our results provide functional evidence that nematode effectors secreted from hypodermis to the parasite cuticle surface target host proteins and *M. incognita* uses MiMIFs to promote parasitism by interfering with the annexin-mediated plant immune responses.

Keywords: Annexin, cuticle, immune response, interaction, macrophage migration inhibitory factor (MIF), *Meloidogyne incognita*, parasitism, plant immunity, root-knot nematode, secretion.

Introduction

Root-knot nematodes (RKNs; *Meloidogyne* spp.) are among the most devastating obligate parasites of plants, causing billions of dollars of agricultural losses worldwide annually (Ibrahim *et al.*, 2011; Jones *et al.*, 2013). The apomictic RKN species *M. incognita*, *M. javanica*, and *M. arenaria* can infect thousands of plant species (Teixeira *et al.*, 2016). Disease development requires the motile RKN pre-parasitic second-stage juveniles (J2s) to penetrate the host root apex and migrate towards the vasculature, where they select root cells and transform them into specialized feeding structures known as 'giant

cells' (Xue *et al.*, 2013; Favery *et al.*, 2016), which serve as the sole source of nutrients for the developing nematode (Caillaud *et al.*, 2008). Like other plant pathogens, RKNs secrete effector proteins into plant cells, to manipulate host cell processes and facilitate parasitism. Several nematode organs can secrete effectors, including the esophageal gland, amphids, phasmids, and hypodermis (Haegeman *et al.*, 2012). Only a few effectors have been detected as secreted *in planta*. Some have been shown to be present in the apoplast *in planta* (Vieira *et al.*, 2011), and three RKN effectors have been shown to target the giant cell nuclei (Jaouannet *et al.*, 2012; Lin *et al.*, 2013; Chen *et al.*, 2017). Like the esophageal gland effectors, cuticular secretions may play an important role in the suppression of plant defense mechanisms (Davies and Curtis, 2011). For example, a functional glutathione peroxidase (GpX) present in the hypodermis can metabolize larger hydroperoxide substrates and probably contributes to the ability of the potato cyst nematode, *Globodera rostochiensis*, to suppress host defenses (Jones *et al.*, 2004). Secreted peroxiredoxins present on the surface of *G. rostochiensis* (Robertson *et al.*, 2000) and in the hypodermis and pseudocoelom of *M. incognita* (Dubreuil *et al.*, 2011) can improve nematode development by scavenging reactive oxygen species (ROS). In addition, a fatty acid- and retinol-binding protein that accumulates at the surface of the *M. javanica* cuticle and is secreted into the surrounding host tissues may play a vital role in promoting nematode parasitism and modulating host defenses (Iberkleid *et al.*, 2013).

Macrophage migration inhibitory factor (MIF) was the first cytokine shown to possess T cell-derived activities involved in the inhibition of macrophage migration (David, 1966). MIF proteins are secreted from cells in a non-conventional secretion pathway, and the secretion of MIF from anterior pituitary cells in response to lipopolysaccharide stimulation suggests that MIF may be a hormone (Bernhagen *et al.*, 1993). MIFs have been shown to have a broad range of biological functions, including an ability to modulate innate and adaptive immune responses, act as a pro-inflammatory cytokine and a chemokine, regulate angiogenesis, apoptosis, and fibrosis, and function as an enzyme with tautomerase and thiol-protein oxidoreductase activity (Calandra and Roger, 2003; Morand *et al.*, 2006; Xu *et al.*, 2013). In animals, there have been many breakthroughs in MIF functional mechanisms. Intracellular signal transduction is initiated by receptor recognition, in which extracellular MIF binds to cell surface protein CD74, along with the potential accessory protein CD44. Sustained extracellular signal-regulated kinases 1 and 2 (ERK1/2) phosphorylation by the MIF–CD74–CD44 complex activates the mitogen-activated protein kinase (MAPK) pathway, which further affects downstream immune responses (Mitchell *et al.*, 1999; Leng *et al.*, 2003; Shi *et al.*, 2006). Meanwhile, MIF could interact with Jun-activation domain-binding protein 1 (JAB1) in the cytosol, antagonize JAB1-controlled pathways, and modulate cellular redox homeostasis (Kleemann *et al.*, 2000; Lue *et al.*, 2007). Furthermore, MIF could interact with two chemokine receptors, CXCR2 and CXCR4, of which CXCR2 also physically interacts with CD74. The complex formed of MIF, CXCR2, and CD74 triggers calcium Ca^{2+} influx and rapid integrin activation (Bernhagen *et al.*, 2007). A recent study showed that MIF is involved in inflammation by interacting with a NOD-like receptor (NLRP3) and mediating the interaction between NLRP3 and the intermediate filament protein vimentin (Lang *et al.*, 2018).

MIF-like proteins from invertebrate species have been shown to be involved in immune escape from hosts. The first nematode MIF homolog was characterized in the filarial parasite *Brugia malayi*, which secretes a MIF-like protein (BmMIF) that can be detected in somatic extracts and in the excretory–secretory products of the parasite, providing the first demonstration that BmMIF could promote parasite survival by modifying host immune responses (Pastrana *et al.*, 1998). A MIF-like protein produced by the hookworm *Ancylostoma ceylanicum*, AceMIF, was shown to bind to the human MIF receptor CD74 and to facilitate infection of larval stages and adult worm survival within the intestine; these findings indicate that AceMIF may act as a virulence factor regulating the host immune response (Cho *et al.*, 2007). Similarly, the filarial parasite *Onchocerca volvulus* secretes MIF-like proteins into the outer cellular covering of the adult worm body, the syncytial hypodermis, and the uterine wall (Ajonina-Ekoti *et al.*, 2013). Recently, a MIF-like protein was reported to be secreted by aphids; this protein acts as a cytokine, modulating host immune responses (Naessens *et al.*, 2015), in a new mechanism of interaction between parasites and plant hosts. However, it remains largely unknown whether and how MIF-like proteins regulate host immune responses or signal transduction during plant–pathogen interactions. Interestingly, plant MIF-like proteins (MDLs) were recently identified, but no functional data are available to date (Panstruga *et al.*, 2015).

Plants have evolved an innate immune system to protect them against various types of attack, in which pathogen-associated molecular pattern (PAMP)-triggered immunity (PTI) and effector-triggered immunity (ETI) play essential roles (Jones and Dangl, 2006; Dangl *et al.*, 2013). The model plant Arabidopsis displays induced immune response-related marker gene expression as part of a response to pathogens (Pieterse *et al.*, 2009; Jaouannet *et al.*, 2013), involving local callose deposition at the site of penetration (Ellinger *et al.*, 2013), and the generation of ROS (Tripathy and Oelmüller, 2012). Many Arabidopsis genes have been implicated in the plant immune system, including those encoding annexins, which act as important regulators of various abiotic and biotic stress responses (Clark *et al.*, 2010; Laohavisit and Davies, 2011). Interestingly, cyst nematodes were reported to secrete annexins to assist parasitism. The beet cyst nematode effector Hs4F01 is an annexin-like protein that interacts with an Arabidopsis oxidoreductase member of the 2-oxoglutarate (2OG)–Fe(II) oxygenase family (Patel *et al.*, 2010). Another cyst nematode annexin-like effector is Ha-ANNEXIN secreted by *Heterodera avenae*, which could suppress host immune responses (Chen *et al.*, 2015). These results highlight the importance of annexins for plant-nematode interactions.

In this study, we characterized *MIF*-like genes from *M. incognita* that are up-regulated upon infection. We showed that MiMIF proteins are secreted into plant tissues and giant cells, thereby promoting parasitism. We chose MiMIF-2 as a representative and found that this protein engaged in physical interactions

with two Arabidopsis annexins, which suppressed host immune responses. Based on these results, we suggest that MiMIF-2 may act as a novel effector interacting with plant annexins to manipulate host immune responses and signal transduction, to promote the survival of parasitic stages of *M. incognita*.

Materials and methods

Nematode culture, plant materials and growth conditions

Meloidogyne incognita strains were reproduced initially from a single egg mass on tomato plants (*Solanum lycopersicum* var.'Baiguo') in a greenhouse at 25 °C. Infective J2s were collected with an improved Baermann funnel for 48–72 h. Different parasitic life stages of the nematode were collected from roots as previously described (Chen *et al.*, 2015). Infected tomato roots were collected at different days after inoculation, cut into 1 cm sections and digested in a mixture of pectase and cellulose (Sinopharm Chemical Reagent Beijing Co., Ltd, China) at 28 °C and 160 rpm overnight. Nematodes were separated under a stereomicroscope.

Surface-sterilized Arabidopsis ecotype Columbia (Col-0) was sown on MS medium (Sigma-Aldrich, USA) as previously described (Quentin *et al.*, 2016). The *AnnAt1* and *AnnAt4* T-DNA mutant lines (*SALK_015426* and *SALK_096465*) were obtained from the Arabidopsis Biological Resource Center (ABRC, USA). Tobacco (*Nicotiana benthamiana*) seeds were grown in pots under conditions of 16 h light and 8 h dark at 23 °C with 60–75% relative humidity.

For *in vivo* nematode infection, Arabidopsis or tomato seedlings were inoculated in soil with 300 J2s per plant. Roots were collected at 35 d post-infection (dpi) and stained using the sodium hypochlorite–acid fuchsine method (Bybd *et al.*, 1983). Egg masses and galls were counted under a dissecting microscope (Olympus, Japan). Juveniles inside roots were isolated by digestion with cellulase. Each experiment was performed three times independently, and 30 plants were counted each time. Data were analysed using Statgraphics Centurion 17 software (Statgraphics Technologies, USA). One-way ANOVA followed by Duncan's *post hoc* test was run to identify significant differences between treatments.

RNA isolation and gene amplification

Meloidogyne incognita mRNA was extracted using a Dynabeads® mRNA DIRECT™ Kit (Invitrogen, USA), and complementary DNA (cDNA) was synthesized using reverse transcriptase SuperScript III (Invitrogen). Arabidopsis total RNA was isolated from seedlings using TRIzol Reagent (Invitrogen) and cDNA was synthesized using M-MLV reverse transcriptase (TaKaRa, Japan). *MIF*-like genes were amplified from cDNA or gDNA of *M. incognita* by PCR using specific primers. The PCR products were cloned into the pMD18-T vector (TaKaRa, Japan) and sequenced. All primers used in this study are listed in Supplementary Table S1 at *JXB* online and were synthesized by TsingKe Biotechnology Co. Ltd, Beijing, China.

Accession numbers and databases used

The predicted nucleotide sequences of *MiMIFs* were obtained from the National Center for Biotechnology Information (NCBI) EST database (http://www.ncbi.nlm.nih.gov/nucest/), and from *Meloidogyne* genomic resources (http://www6.inra.fr/meloidogyne_incognita/). Multiple amino acid sequence alignment analyses of MIF-like proteins from *B. malayi*, Arabidopsis, *Homo sapiens*, *M. hapla*, *M. incognita*, *Ascaris suum*, *A. ceylanicum*, *O. volvulus*, *Caenorhabditis elegans*, and *Plasmodium falciparum* were conducted using DNAMAN V6 (Lynnon Biosof, USA). All accession numbers are listed in Supplementary Table S2.

Developmental expression analysis and RT-qPCR analysis

Illumina transcriptomic data obtained during developmental stages (eggs, pre-parasitic J2s, parasitic juveniles, and adult females) were described recently (Blanc-Mathieu *et al.*, 2017). Real-time quantitative PCR (RT-qPCR) was performed on an ABI Prism 7000 real-time PCR system (Applied Biosystems, USA). *Meloidogyne incognita tubulin* was used as an internal control. RT-qPCR was conducted using a SYBR Premix Ex Taq (TaKaRa, Japan) under standard conditions. The results were analysed using the $2^{-\Delta\Delta C_t}$ method (Livak and Schmittgen, 2001).

Anti-MiMIF-2 polyclonal antibody production and immunolocalization

Recombinant MiMIF-2 (rMiMIF-2, with an N-terminal His tag) was purified using QIA*express*® Ni-NTA Fast Start (Qiagen, Germany). Protein concentration and purity were determined by the BCA Protein Assay Kit (Beijing ComWin Biotech Co., Ltd, China) and by SDS-PAGE. The anti-MiMIF-2 polyclonal serum was purified from immunized rabbits (Beijing Protein Innovation Co., Ltd, Beijing, China). Western blotting was conducted to verify the antibody specificity. The *MiMIF-2* mutant (r*MiMIF*-2-mu; N-terminal Pro1→Gly1) was generated by PCR.

Ultrastructural immunocytochemistry was performed as previously described (Dubreuil *et al.*, 2011). Freshly hatched J2s were fixed with 4% paraformaldehyde (PAF) or 4% PAF and 0.2% glutaraldehyde (PG) in 0.1 M phosphate buffer (pH 7.4). J2s were dehydrated in an ethanol series and embedded in acrylic resin (LR-White) before sectioning and immunogold labelling. The anti-MiMIF-2 antibody (1:200) and protein A–gold (PAG) of 15 nm (1:50) were used. For controls, sections were processed according to the same procedure excepted that the primary antibody was omitted. Eighty-nanometer ultrathin sections were contrasted with 4% uranyl acetate in water and visualized using a JEM 1400 electron microscope operating at 100 kV equipped with a Morada SIS camera. For immunohistochemistry on sections of tomato galls, we used the protocol previously described (de Almeida Engler *et al.*, 2004). Tomato galls were fixed in 8% formaldehyde, dehydrated and embedded in butyl-methylmethacrylate. MiMIF-2 antibody and secondary antibody (goat anti-rabbit Alexa Fluor 488 conjugate antibody, Molecular Probes) were diluted 250- and 300-fold in blocking solution, respectively. Nuclei were stained by 4′,6-diamidino-2-phenylindole (DAPI) (Sigma-Aldrich). Images were captured by confocal microscopy (Zeiss LSM880, Germany).

In planta RNAi and generation of transgenic Arabidopsis plants

For RNAi experiments, two *MiMIF-2* fragments (1–339 bp) were amplified and cloned in the forward and backward pSAT5 intron, and then inserted into pSuper-RNAi (Dafny-Yelin *et al.*, 2007). For ectopic expression, the open reading frames (ORFs) of *MiMIF-2*, *AnnAt1* (*At1g35720*) and *AnnAt4* (*At2g38750*) were amplified and inserted into Super1300-FLAG. The vectors were transformed into *Agrobacterium tumefaciens* GV3101 and used for transformation of Arabidopsis via the floral dip method (Zhang *et al.*, 2006). Homozygous T3 plants were confirmed by RT-PCR and western blotting.

Cell-death suppression assay in N. benthamiana, callose staining and defense gene expression analyses

The coding regions of *MiMIF-2* and *GFP* were amplified and cloned into PVX vector pGR107 with a FLAG-tag fused at the N-terminus or a HA-tag fused at the C-terminus and transformed into *A. tumefaciens* GV3101. *Agrobacterium tumefaciens* cells carrying BAX or RBP1/Gpa2 were used to trigger cell death in *N. benthamiana* leaves (Sacco *et al.*, 2009; Jing *et al.*, 2016). Agro-infiltrations into 4-week-old *N. benthamiana* leaves were performed as described in Nguyen *et al.* (2018).

For callose deposition assay, Arabidopsis leaves from 4-week-old *MiMIF-2* lines and wild type (WT, Col-0) were treated with 1 μM flg22 or buffer for 24 h. Samples were stained with aniline blue for 3 h and then examined under a photomicroscope.

Defense suppression test was conducted as described previously (Jaouannet *et al.*, 2013). To analyse defense gene expression, 10-day-old seedlings of *MiMIF-2*-expressing line and WT were treated with 1 μM flg22. The expression of the defense marker genes *PR1*, *PR3*, *FRK1*, *CYP81*, *RbohD*,

and *RbohF* was determined by RT-qPCR. Arabidopsis ubiquitin carboxyl terminal hydrolase 22 (*UBP22*) was used as an internal control.

Arabidopsis protein immunoprecipitation (IP) experiments and LC-MS/MS analysis

For the IP experiments, Arabidopsis total protein was extracted from *MiMIF-2-FLAG*-expressing lines (three different lines) and WT plants. IP was performed using the anti-FLAG M2 affinity gel resin (Sigma-Aldrich). The beads were washed twice with 1 ml of ice-cold phosphate-buffered saline (PBS), followed by the immediate addition of 1 ml protein solution and incubation at 4 °C for 4 h. The resin was thoroughly washed five times with 1 ml of ice-cold PBS, and then the proteins were eluted for analysis. A Q-Exactive nanospray ESI-MS mass spectrometer (Thermo, USA) was used for liquid chromatography–tandem mass spectrometry (LC-MS/MS) at China Agricultural University Functional Genomics Platform. The acquired mass spectrometric data were pre-analysed using Mascot Distiller 2.4 (UK) and then anatomized to search an NCBI non-redundant protein database and the Swiss-prot database.

Subcellular localization, bimolecular fluorescence complementation in planta *and aequorin-based* $[Ca^{2+}]_{cyt}$ *measurement*

The open reading frame of *MiMIF-2* without stop codon was amplified and cloned into the p35S-eGFP vector with an enhanced green fluorescent protein (eGFP) fused at the C-terminus. For bimolecular fluorescence complementation (BiFC) assay, full-length candidate genes or *MiMIF-2* coding sequences were amplified and cloned into the binary vectors pSPYNE and pSPYCE, respectively (Walter *et al.*, 2004). The constructs were transformed into *A. tumefaciens* strain EHA105. Four-week-old *N. benthamiana* leaves were agro-infiltrated and images were captured by laser confocal fluorescence microscopy (Leica SP8, Germany) at an excitation wavelength of 515 nm.

Aequorin/MiMIF-2 transgenic lines were generated from a cross between the *aequorin* line (Laohavisit *et al.*, 2009) and *MiMIF-2* transgenic lines. The *aequorin-annAt1* and *aequorin-annAt4* seeds were gifts from Yan Guo's lab. Ten-day-old *aequorin*-expressing seedlings were used for measurements of root $[Ca^{2+}]_{cyt}$ according to a previously described method (Laohavisit *et al.*, 2012). Roots were suspended in aequorin buffer (5 mM KCl, 2 mM $CaCl_2$, and 2 mM Tris/MES, pH 5.7, with 10 μM coelentrazine) for 5 h in the dark (25 °C), washed with osmotically adjusted aequorin buffer without coelentrazine, and resuspended in this buffer (100 μl), and left in the dark for 30 min. The baseline luminescence was recorded for 60 s, followed by the addition of 100 μL of buffer (20 mM H_2O_2). Luminescence was recorded every second for 120 s. Discharge buffer was then injected (final concentration: 10% (v/v) ethanol, 1 M $CaCl_2$), and the luminescence was recorded for an additional 120 s.

In vivo co-immunoprecipitation assay

For a co-immunoprecipitation (Co-IP) assay, the coding regions of *AnnAt1*, *AnnAt4*, or *MiMIF-2* were cloned into the PVX vector pGR107 with a FLAG-tag fused at the N-terminus and a HA-tag fused at the C-terminus, respectively, and then transformed into *A. tumefaciens* GV3101. *Nicotiana benthamiana* leaves were used for co-expressing MiMIF-2 and annexins using the above-described method. Co-IP was conducted as previously described (Liu *et al.*, 2017), and SDS-PAGE loading buffer (1×) was added to the beads and heated at 100 °C for 10 min to elute the proteins. The eluted proteins were subsequently subjected to immunoblotting using anti-FLAG (Sigma-Aldrich) and horseradish peroxidase (HRP)-conjugated anti-HA antibodies (Roche, USA), respectively.

Protein extraction and western blotting

Total proteins were extracted from 2 dpi agro-infiltrated *N. benthamiana* leaves or Arabidopsis seedlings using a protein extraction kit (Beijing ComWin Biotech Co., Ltd, China). For western blot, the primary antibody (anti-FLAG or anti-HA, Sigma-Aldrich) was used at 1: 5000. For immunoblot analysis of MAPK activation, 10-day-old Arabidopsis seedling samples were collected after treatment with 1 μM flg22. A phospho-44/42 MAPK (ERK1/2) polyclonal antibody (Cell Signaling Technology, USA) diluted 1:2000 and an anti-rabbit secondary antibody diluted 1:8000 were used. The protein was detected with the eECL Western Blot Kit (Beijing ComWin Biotech Co., Ltd, China).

Results

Identification of M. incognita MIF*-like genes and their expression in different life stages*

Our searches of the NCBI EST database and *M. incognita* genome sequences (Abad *et al.*, 2008; Blanc-Mathieu *et al.*, 2017) identified four genes encoding MIF-like proteins: *MiMIF-1* (Vermeire *et al.*, 2008), *MiMIF-2*, *MiMIF-3*, and *MiMIF-4*. These genes are organized in tandem arrays on two scaffolds. *MiMIF-1* and *MiMIF-2*, and *MiMIF-3* and *MiMIF-4* share 97–98% nucleotide sequence identity, whereas *MiMIF-1/MiMIF-2* and *MiMIF-3/MiMIF-4* only share about 82% sequence identity (Fig. 1A; Supplementary Fig. S1A). The *MiMIF-1* gene has a single base-pair deletion in position 260 (Supplementary Fig. S1A, indicated by black arrow), resulting in the premature termination of translation at bp 285 (Supplementary Fig. S1A, indicated by red frame), leading to a protein truncated by 19 amino acids (aa). Interestingly, *MiMIF-3* and *MiMIF-1* form an operon and are transcribed together to generate a single mRNA strand (Supplementary Fig. S1B, C). Sequence alignment showed that *MiMIF*-1 (94 aa), *MiMIF*-2 (113 aa), *MiMIF*-3 (112 aa), and *MiMIF*-4 (112 aa) were 75–99% identical (Fig. 1A; Supplementary Fig. S1D). They all contain three conserved residues (Pro1, Lys32, and Ile64) of the active sites for tautomerase activity identified in human MIF (Fig. 1B, black triangle), but *MiMIF* sequences lacked the Val106 residue (Fig. 1B, red triangle) for tautomerase activity and the C-X-X-C motif found in the thioredoxin superfamily of thiol-protein oxidoreductases (Fig. 1B).

The nucleotide sequences of the four *MiMIFs* displayed a high level of identity, and *MiMIF-3* and *MiMIF-1* were found to be cotranscribed (Supplementary Fig. S1A, B), making it difficult to study individual *MiMIF* expression profiles. However, Illumina transcriptomic data obtained during developmental stages (eggs; pre-parasitic J2s; parasitic juveniles and adult females) (Blanc-Mathieu *et al.*, 2017) revealed higher levels of *MiMIFs* expression in parasitic juveniles than in pre-parasitic J2s (Fig. 1C).

MiMIFs are localized in the hypodermis and cuticle, and secreted into plants and accumulated in giant cells

To analyse the tissue localization of MiMIFs and demonstrate that MiMIFs are secreted into host-plant tissues, we produced a polyclonal antibody against rMiMIF-2. On western blots, this polyclonal antibody specifically detected rMiMIF-2 and MiMIFs in total proteins from pre-parasitic J2s at the expected size of ~13 kDa (Supplementary Fig. S2). No signal was detected in total proteins from tomato roots or leaves. Ultrastructural immunocytochemistry analyses with the polyclonal antibody were performed on pre-parasitic J2s. MiMIF proteins were

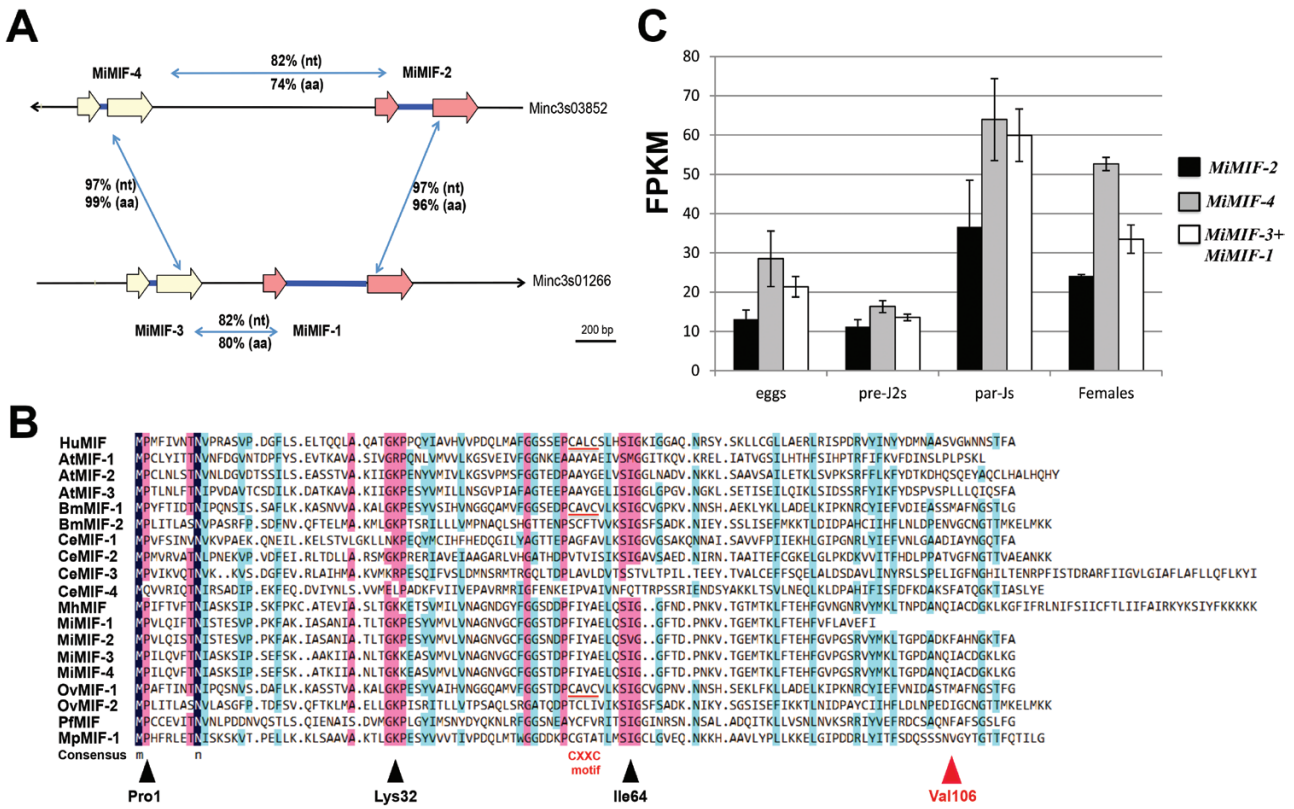

Fig. 1. *Meloidogyne incognita MIF*-like genes are more strongly expressed in parasitic stages. (A) Organization of *MIF* genes in the *M. incognita* genome. Exons are represented by arrows, introns by blue lines. The *M. incognita* scaffolds and the percentage nucleotide/amino acid identity between the ORFs/proteins are indicated. (B) Alignment of the deduced amino-acid sequences of the MIF-like proteins from *M. incognita*, *Brugia malayi*, Arabidopsis, *C. elegans*, *Plasmodium falciparum*, *Onchocerca volvulus*, *Meloidogyne hapla*, *Myzus percicae*, and humans. Identical amino acids are shown in black, highly similar (>75%) amino acid residues are shown in pink, and similar (>50%) amino-acid residues are shown in blue. Triangles (black and red) indicate the tautomerase active site residues conserved in mammalian MIF-like proteins; black triangles are tautomerase active site residues that exist in MiMIFs; red line, C-X-X-C motif. (C) Developmental expression profile of *MiMIF*s. The mean gene expression is presented as fragments per kilobase of transcript per million mapped reads (FPKM) values and were calculated from three independent biological samples for each developmental stage: eggs, pre-parasitic second-stage juveniles (pre-J2), and parasitic juveniles and females (par-Js). Data are presented as means ±SEM.

mostly detected in the hypodermis in contact with the cuticle, in the cuticle, in the pseudocoelom surrounding the stylet, and barely in the muscle (Fig. 2A, B; Supplementary Fig. S3). No gold particles (black dots) were observed in control treatments (Fig. 2C). Immunohistochemistry analyses were performed on gall sections from tomato plants 15 d post-infection (dpi) with *M. incognita*. Fluorescence was observed around the nematode head and cuticle adjacent to the surrounding host cells (Fig. 2D, E; Supplementary Fig. S4). This result indicates secretion into and accumulation of MiMIFs in the intercellular space between the nematode body and the host cells. Moreover, several giant cells showed a clear signal at the cytoplasmic level and in particular near the plasma membrane (Fig. 2G, H). In control experiments with secondary antibody only, no signal was observed on sections of infected roots at similar time points (Fig. 2F, I). Thus, MiMIFs are secreted *in planta* from *M. incognita* hypodermis to the parasite surface during parasitism and are able to target the giant cells.

In planta *RNAi of* MiMIFs *affects nematode parasitism*

We assessed the role of *MiMIF* genes during parasitism by silencing *MiMIFs in planta* through host-derived RNAi. Four homozygous Ri-T3 transgenic Arabidopsis lines expressing the *MiMIF-2* full-length coding sequence (CDS) hairpin double-stranded RNA (dsRNA; 339 bp in pSuper vector; the identical phenotypes of different lines are shown in Supplementary Fig. S5) and two *GFP* hairpin dsRNA lines were obtained. *MiMIFs* transcript abundance was assessed in parasitic nematodes extracted at 14 dpi, and was found to be strongly reduced (64% to 80%) in the four Ri-T3 lines compared with control lines (Fig. 3A), demonstrating the efficacy of host-derived RNAi-mediated gene silencing. At 35 dpi, the numbers of galls and nematodes were about 60% lower ($P<0.05$) in Ri-T3 plants than in plants treated with the *GFP* control lines (Fig. 3B). Similar results were obtained in three independent trials. These findings suggest that *MiMIFs* play a key role in root-knot nematode parasitism.

MiMIF-2 *expression in Arabidopsis increases susceptibility to* M. incognita

We showed that native *MiMIF*s were indeed delivered into the cytoplasm of host cells and we then expressed *MiMIF-2* ectopically in transformed Arabidopsis lines. Transgenic plants were verified by RT-PCR; the phenotype of three independent

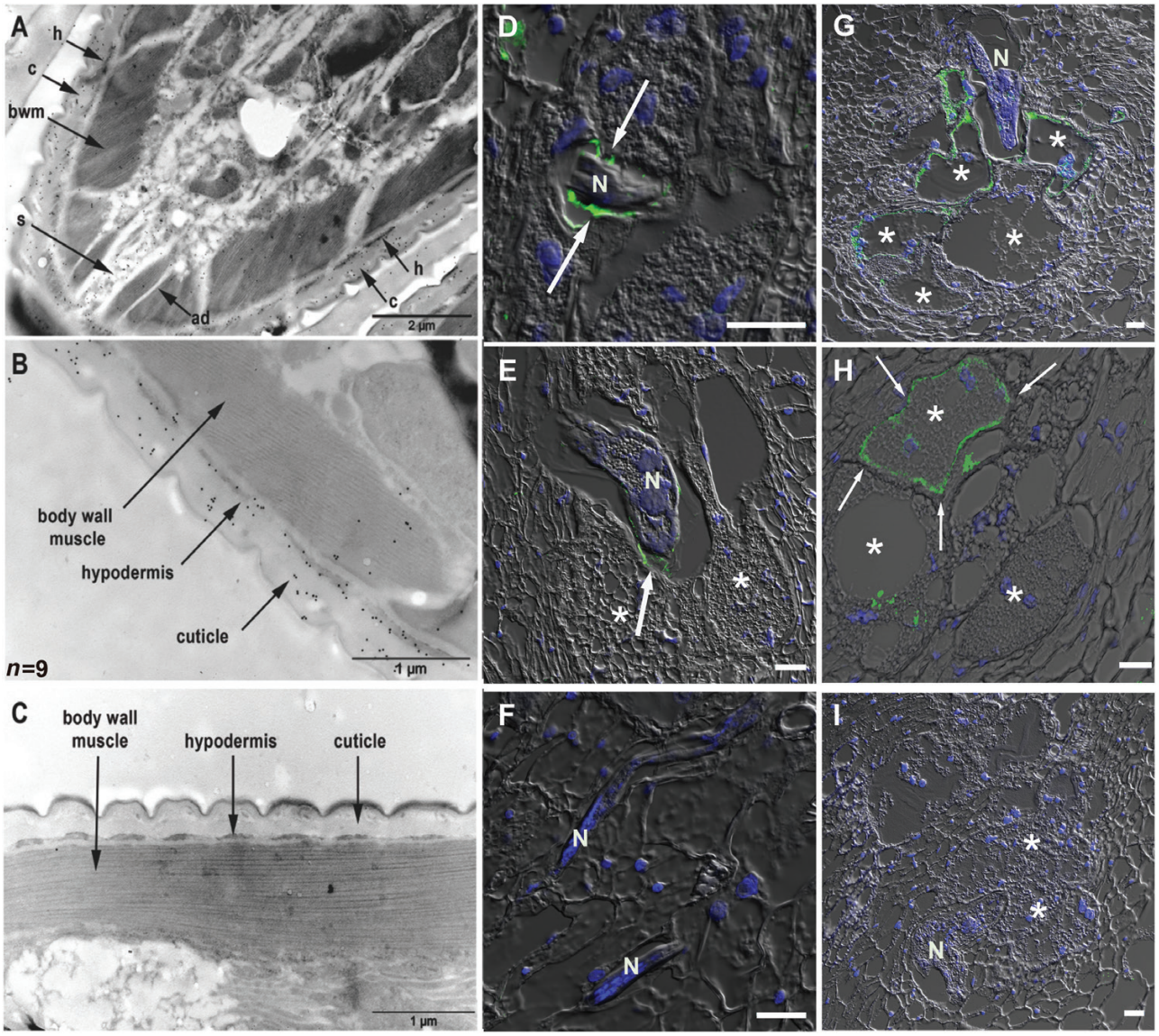

Fig. 2. Localization of MiMIF proteins in nematodes and *in planta*. (A, B) Ultrastructural immunocytochemistry of *M. incognita* MIF proteins. Section of the head and anterior part of a pre-J2 fixed in 4% paraformaldehyde (PAF) or 4% PAF and 0.2% glutaraldehyde (PG) showing MIF protein accumulations in the hypodermis (h) and in the cuticle (c), and also detected in the body wall muscle (bwm) and in the pseudocoelom surrounding the stylet (s). ad, amphid. *n*=9 indicates the number of similar results. (C) Control sections of J2s fixed in PG or PAF without anti-MiMIF-2 antibody. (D–I) Immunodetection of the MiMIF proteins in tomato gall sections. Tomato roots were fixed into methylacrylate after infection with *M. incognita* for 15 d. The anti-MiMIF-2 antibody (1:250) was applied on gall sections. Alexa Fluor 488-conjugated secondary antibody was used to detect the fluorescence. (D, E) MiMIF proteins accumulated along the nematode cuticle and adjacent plant tissues surrounding the nematode head. (F) Galls containing parasitic J2 nematodes incubated only with secondary antibody as a negative control, showing no signal. (G) Signal was observed around nematode head and in giant cells near the plasma membrane. (H) Signal was detected around the giant cell and nucleus. (I) Galls containing nematode and giant cells incubated only with secondary antibody as a negative control, showing no signal. Micrographs (E, F, G, H) are overlays of images of the differential interference contrast, Alexa Fluor 488-conjugated secondary antibody and DAPI-stained nuclei. Individual images are listed in Supplementary Fig. S3. N, nematode; *, giant cell. Scale bars 20 µm for images (D–I). White arrows indicate the MiMIF-2 fluorescence.

homozygous T3 lines expressing *MiMIF-2-FLAG* (lines OE-T3-3, OE-T3-4, and OE-T3-5) showed no obvious difference compared with WT plant, and the presence of a 13 kDa MiMIF-2-FLAG protein was confirmed by western blotting (Supplementary Figs S5, S6). Infection assays with *M. incognita* showed that all three transgenic lines were significantly ($P<0.05$) more susceptible than WT to *M. incognita* infection (Fig. 3C). The transgenic lines had up to 30% more galls and parasitic nematodes at 35 dpi. Similar results were obtained in three independent biological tests, each with 30 plants.

MiMIF-2 *suppresses defense responses in plants*

As the expression of *MiMIF-2* in Arabidopsis enhanced *M. incognita* infection, we investigated whether MiMIF-2 may regulate plant immune responses. We first tested whether MiMIF-2 has the ability to suppress programmed cell death (PCD) induced by proapoptotic BAX or *Globodera* RBP-1/Gpa2 resistance protein. BAX and RBP-1/Gpa2 constructs were agroinfiltrated 24 h after tagged MiMIF-2 or controls into *N. benthamiana* leaves, respectively. BAX-induced PCD was completely suppressed when the leaves were infiltrated with

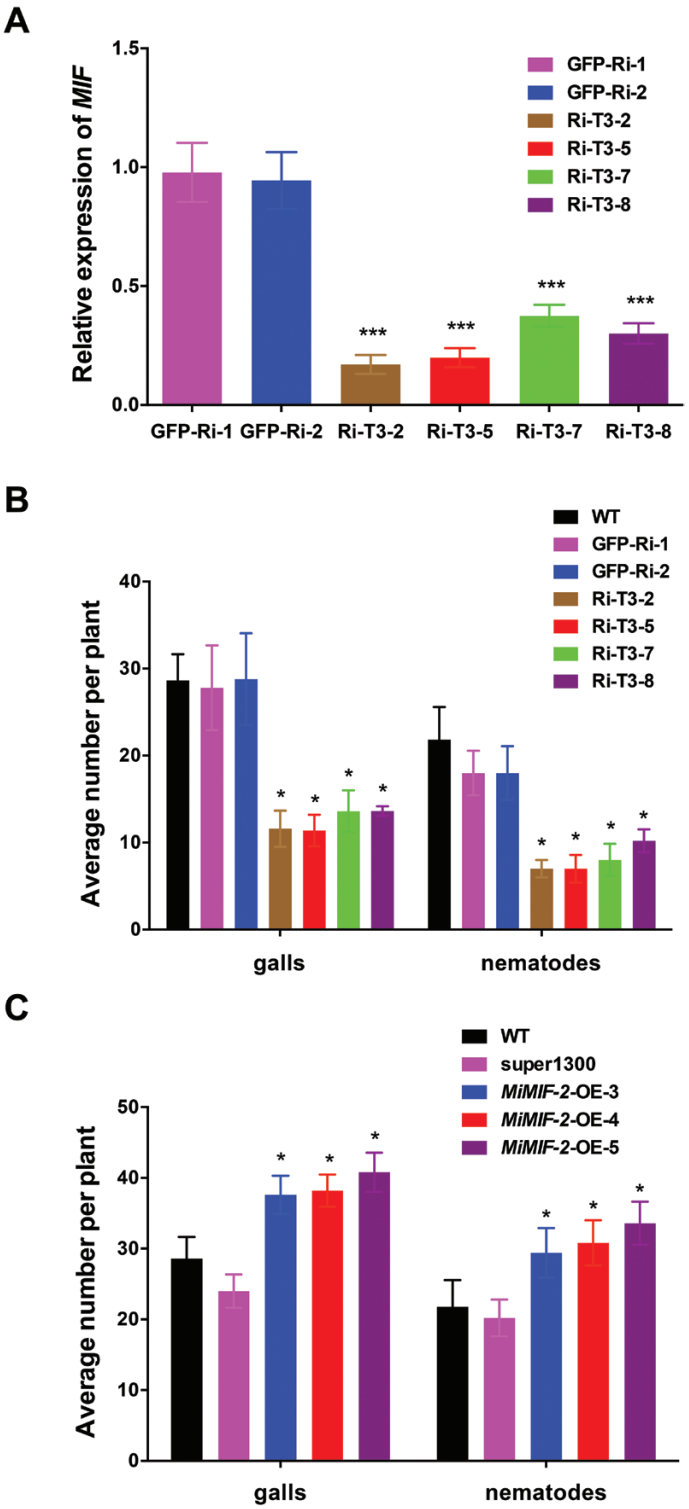

Fig. 3. The effect of *MiMIF-2* silencing and expression *in planta* on *M. incognita* parasitism. (A) RT-qPCR assays showed the level of *MiMIF* expression in *M. incognita* collected from Arabidopsis lines (*GFP* RNAi lines and *Mimif-2* RNAi lines) treated by host-derived RNAi *in planta*, 14 d post-inoculation (dpi). The *tubulin* gene was used as an internal control. (B) The total numbers of galls and nematodes were counted at 35 dpi in the *Mimif-2* RNAi Ri-T3 lines (Ri-T3-2, -5, -7, and -8). (C) *MiMIF-2* expression in Arabidopsis increases susceptibility to *M. incognita*. The total numbers of galls and nematodes were counted at 35 dpi in *MiMIF-2* ectopically expressing lines (*MiMIF*-2-OE-3, -4, and -5). Data are presented as means ±SD ($n \geq 30$). Asterisks denote significant differences (*$P<0.05$; ***$P<0.001$, one-way ANOVA). All experiments were performed three times with similar results, and at least 30 plants were analysed per line. (This figure is available in color at *JXB* online.)

A. tumefaciens cells carrying FLAG–MiMIF-2 but not with FLAG–GFP (Fig. 4A, B). Moreover, we found that MiMIF-2–HA could suppress cell death triggered by Gpa2/RBP-1 (Fig. 4C, D). Msp40, a *M. incognita* effector, was used as negative control (Niu *et al.*, 2016) and did not suppress cell death triggered by Gpa2/RBP-1.

We next investigated whether MiMIF-2 affected PAMP-triggered immunity (PTI). PTI requires signal transduction from receptors of downstream components via MAPK cascades. We compared the MAPK cascades of WT Arabidopsis and *MiMIF-2*-OE-T3 plants, by monitoring levels of activated phosphorylated MAPKs, MPK3 and MPK6, after treatment with the bacterial PAMP flg22 (flagellin-derived peptide), with a polyclonal α-phospho-44/42 MAPK (ERK1/2) antibody. The activation of MPK3 and MPK6 by flg22 was significantly weaker in *MiMIF-2*-OE-T3 seedlings than in WT seedlings (Fig. 5A). We analysed the expression of six defense marker genes (*PR1*, *PR3*, *FRK1*, *CYP81*, *RbohD*, and *RbohF*) after treatment with flg22. As expected, flg22 significantly induced the expression of five defense marker genes (*PR1*, *PR3*, *FRK1*, *CYP81*, and *RbohD*) in WT plants, but not *RbohF*. By contrast, these five marker genes were repressed in *MiMIF-2*-OE-T3 plants, and this repression was particularly strong for *CYP81* (Fig. 5B). Moreover, flg22 induced almost no callose deposition in *MiMIF-2*-OE plants, contrasting with its effects on WT cotyledons ($P<0.001$, Fig. 5C, D).

MiMIF-2 *interacts with AnnAt1 and AnnAt4* in vivo

We identified the target proteins of MiMIF-2 by performing liquid *in planta* immunoprecipitation (IP) followed by LC-MS/MS analysis on the three *MiMIF*-2-OE lines and WT Arabidopsis. We focused on candidate proteins that specifically pulled down in the three *MiMIF*-2-OE plants but not in the WT control (Supplementary Table S3). We then examined the interactions between these candidates and MiMIF-2 using BiFC assays and validated annexin AnnAt1 (AT1G35720) as a MiMIF-2 target. The co-expression of MiMIF-2–nEYFP and AnnAt1–cEYFP in tobacco leaves reconstituted yellow fluorescent protein (YFP) activity in the cytoplasm of transformed cells (Fig. 6A; Supplementary Fig. S7), whereas no YFP fluorescence was observed in YFP plasmids containing control constructs. These results constitute the first validation of AnnAt1 and MiMIF-2 interaction.

Eight annexins have been described in Arabidopsis (Clark *et al.*, 2001; Cantero *et al.*, 2006). We investigated whether MiMIF-2 could interact with other annexins that are strongly expressed in roots (AnnAt2, AnnAt3, AnnAt4, AnnAt5, AnnAt8) by using BiFC. We found that only AnnAt4 (AT2G38750) interacted with MiMIF-2 (Fig. 6A; Supplementary Fig. S8). Following agroinfiltration into *N. benthamiana* leaves, AnnAt–GFP and AnnAt4–GFP localized in the cytoplasm (Supplementary Fig. S9), whereas MiMIF-2 was found in the cytoplasm and the nuclei (Supplementary Fig. S10), consistent with interactions between these proteins occurring in the cytoplasm.

To validate these interactions, Co-IP was performed in *N. benthamiana*. FLAG–AnnAt1 or FLAG–AnnAt4 and MiMIF-2–HA were co-expressed in plants. As a negative control, tobacco leaves were co-infiltrated with FLAG–GFP

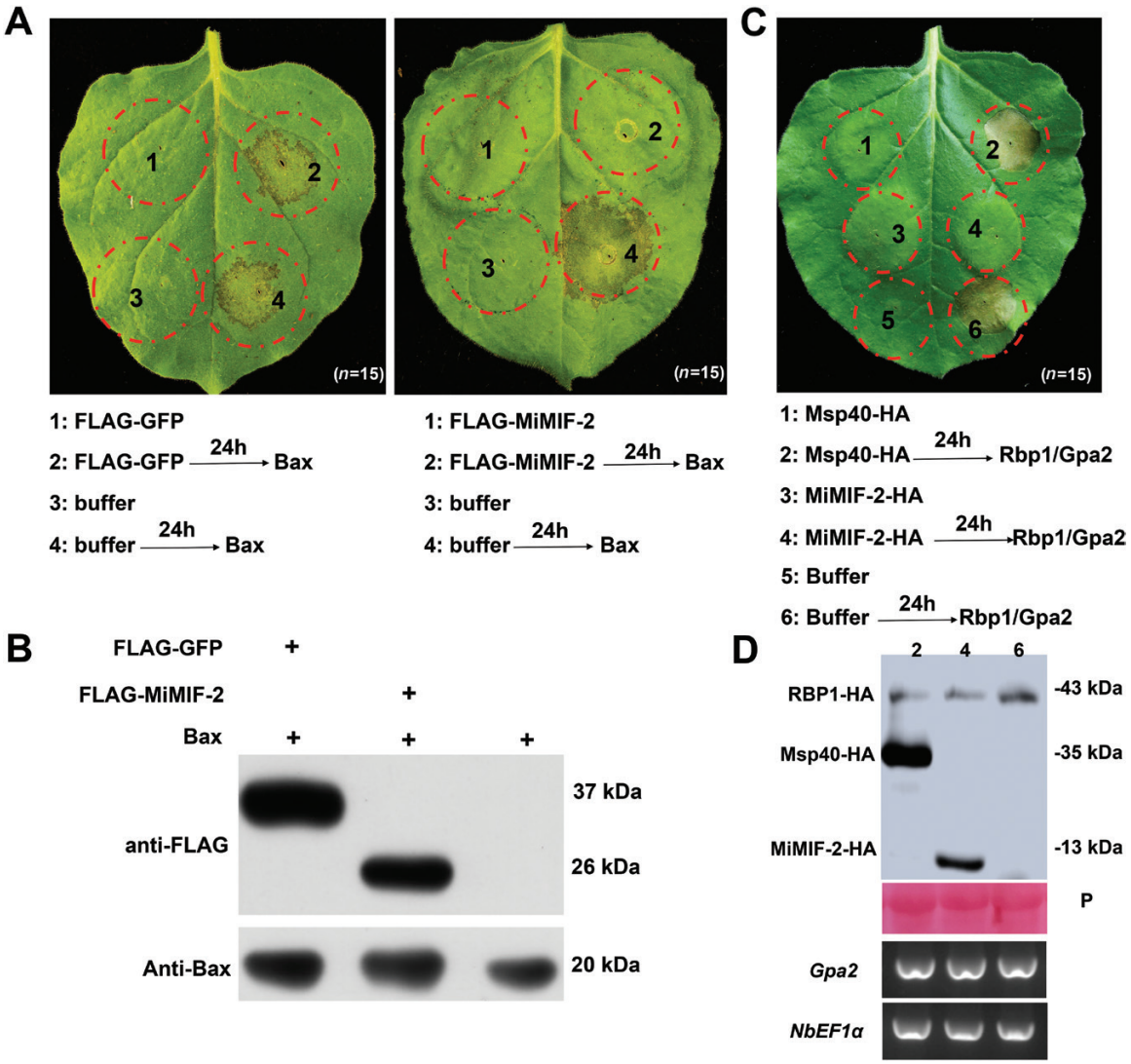

Fig. 4. MiMIF-2 suppressed BAX- and RBP1/Gpa2-induced programmed cell death (PCD) in *N. benthamiana*. (A) FLAG-MiMIF-2 suppressed BAX-induced PCD. *Nicotiana benthamiana* leaves were infiltrated with *A. tumefaciens* carrying the corresponding constructs, and the cell death photographs were taken at 5 dpi (5 plants and infiltrate 3 leaves of each plant, *n*=15). (B) For suppressing BAX-induced cell death, the presence of MiMIF-2, GFP, and BAX protein was confirmed by immunoblotting with anti-FLAG or anti-BAX antibodies. (C) MiMIF-2-HA suppressed RBP1/Gpa2-induced PCD. *Nicotiana benthamiana* leaves were infiltrated with *A. tumefaciens* carrying the corresponding constructs, and the cell death photographs were taken at 5 dpi. *n* indicates similar leaf phenotype in each experiment (5 plants and infiltrate 3 leaves of each plant). (D) For suppressing RBP1/Gpa2-triggered cell death, the presence of MiMIF-2-HA, Msp40-HA, and RBP1-HA protein was detected by immunoblotting with anti-HA antibody. The expression of *Gpa2* was confirmed by RT-PCR; *N. benthamiana* translation elongation factor 1α (*NbEF1α*) was used as internal control. (This figure is available in color at *JXB* online.)

and MiMIF-2–HA. An anti-FLAG antibody clearly detected single target bands at 37 and 27 kDa, corresponding to the expected sizes of AnnAt1 and AnnAt4, and eGFP, respectively. Analyses of the immunoprecipitated proteins with HA antibody showed that MiMIF-2 (13 kDa) was specifically pulled down by AnnAt1 and AnnAt4, but not by eGFP (Fig. 6B).

The entire MiMIF-2 structure and the Ca^{2+}-binding sites of annexins are required for interaction

The amino-terminal proline residue of MIF is crucial for its biochemical activities (Calandra and Roger, 2003). Likewise, annexins contain Ca^{2+}-binding sites of functional importance (Gerke and Moss, 2002; Laohavisit and Davies, 2009). We investigated the possible involvement of these sites in protein–protein interactions, by generating a series of mutations in the protein sequences of MiMIF-2, AnnAt1, and AnnAt4 (Fig. 7A). A missense mutant (P2/G, MiMIF-2-mu) and a deletion mutant (MiMIF-2-113aa) were generated in the BiFC and Co-IP vectors. Four missense mutations with amino-acid substitutions affecting the Ca^{2+}-binding sites of AnnAt1 (AnnAt1E68A, AnnAt1D299A, and AnnAt1E68A/D299A) and AnnAt4 (AnnAt4E72A) were also constructed. The BiFC and Co-IP assays clearly showed that the entire structure of MiMIF-2, including, in particular, the amino-terminal proline residue, was required for interaction with AnnAt1 and AnnAt4 (Fig. 7B, D). The Ca^{2+}-binding sites of AnnAt1 and AnnAt4 were also essential for interaction with MiMIF-2 (Fig. 7C, D).

AnnAt1 and AnnAt4 are involved in Arabidopsis response to M. incognita

We investigated the biological functions of AnnAt1 and AnnAt4 in mediating the response to *M. incognita* by manipulating the

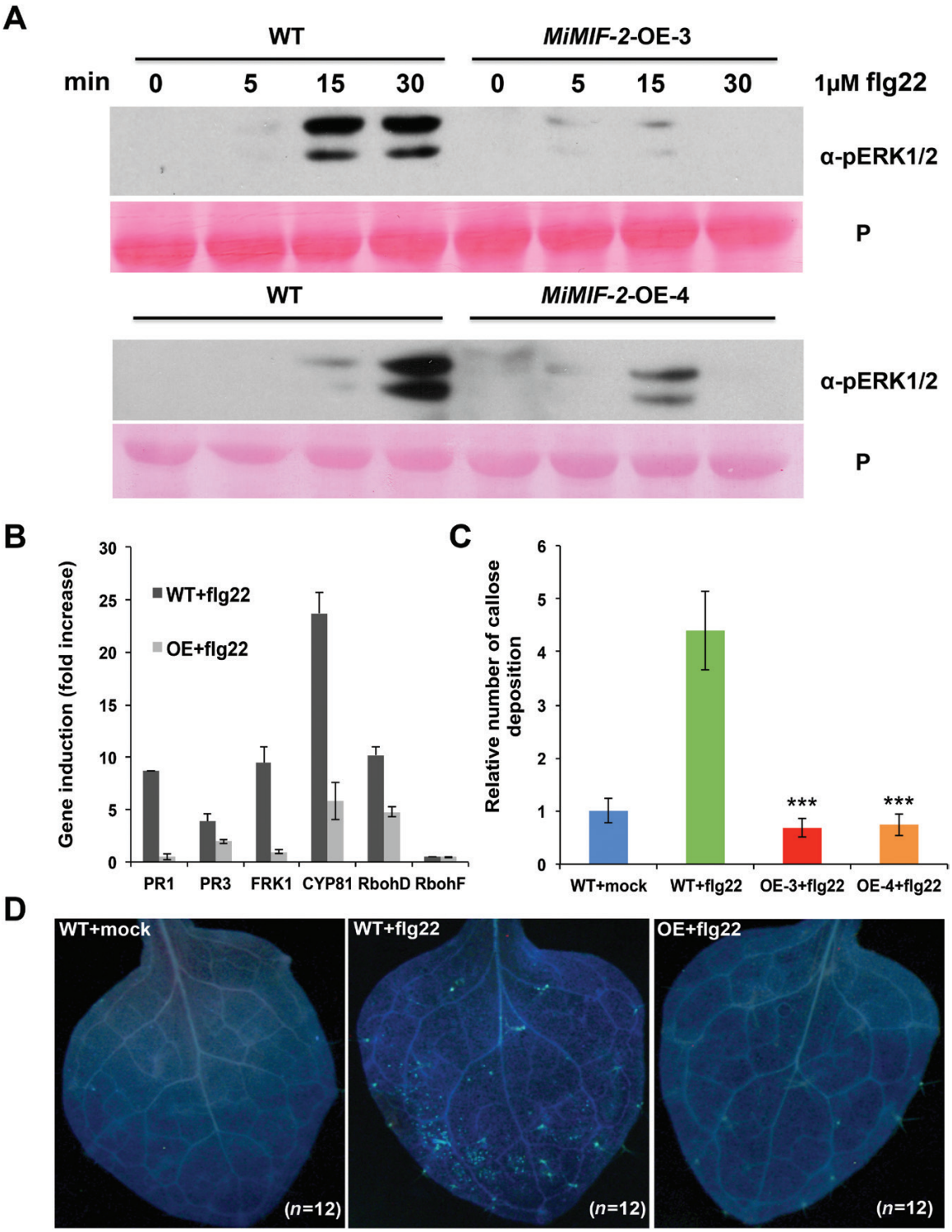

Fig. 5. MiMIF-2 suppresses the defense triggered by flg22 in Arabidopsis. (A) MiMIF-2 suppresses the pathogen-associated molecular pattern (PAMP)-triggered immunity (PTI) response induced by flg22 in Arabidopsis. Twelve-day-old seedlings of wild-type plants (WT) and plants expressing *MiMIF*-2 (*MiMIF*-2-OE-3 and *MiMIF*-2-OE-4) were treated with 1 μM flg22. MAPK activation was analysed by western blotting with an α-phospho-p44/42 MAPK antibody (Cell Signaling Technology, USA). P, Ponceau S staining of the membrane, demonstrating equal protein loading. (B) WT and *MiMIF*-2 (*MiMIF*-2-OE-3 and *MiMIF*-2-OE-4) seedlings were grown for 10 d on MS agar and treated with 1 μM flg22. Induction of the defense marker genes *PR1*, *PR3*, *FRK1*, *CYP81*, *RbohD*, and *RbohF* in response to flg22 was assessed by RT-qPCR and comparison with plants grown without flg22 treatment. (C, D) Callose deposition in the cotyledons of 10-day-old Arabidopsis seedlings from WT and *MiMIF*-2-expressing plants (*MiMIF-2-OE-3* and *MiMIF-2-OE-4*) 24 h after mock or 1 μM flg22 treatment. Callose deposition was analysed by staining with aniline blue, images were captured by UV epifluorescence microscopy, and ImageJ was used to determine the number of fluorescent spots. Error bars represent the mean ±SD (n=12), and asterisks denote significant differences (***P<0.001, one-way ANOVA). All these experiments were repeated three times with similar results. (This figure is available in color at *JXB* online.)

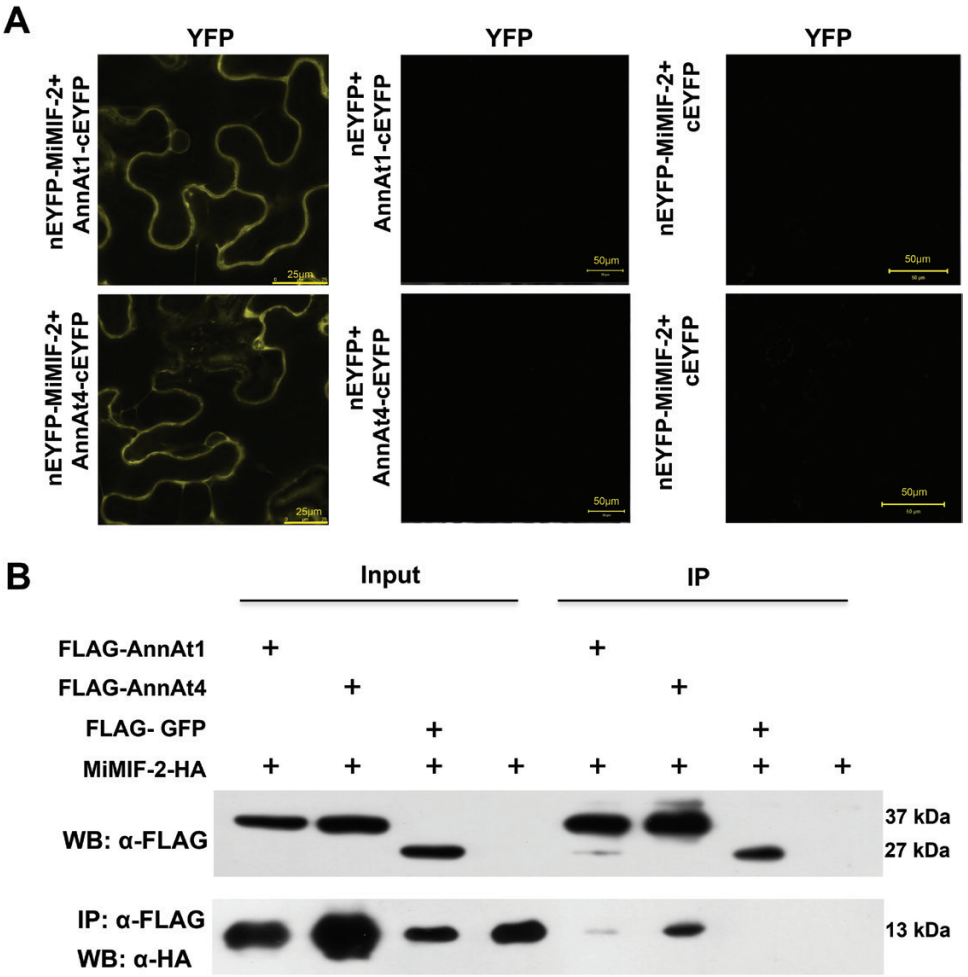

Fig. 6. MiMIF-2 interacts with two Arabidopsis annexins, AnnAt1 and AnnAt4. (A) Bimolecular fluorescent complementation (BiFC) visualization of the MiMIF-2–annexin interaction. nEYFP–MiMIF-2 and AnnAt1–cEYFP or AnnAt4–cEYFP were co-expressed in tobacco leaves. Controls were performed by co-expressing nEYFP and AnnAt1–cEYFP, nEYFP and AnnAt4–cEYFP, and nEYFP–MiMIF-2 and cEYFP. Images were obtained 36 h after co-expression. YFP, yellow fluorescent protein. Bars, 25 or 50 μm as shown. (B) Co-immunoprecipitation of AnnAt1 or AnnAt4 with MiMIF-2. AnnAt1–FLAG, AnnAt4–FLAG or GFP–FLAG was transiently co-expressed with MiMIF-2–HA in tobacco leaves. The Co-IP experiment was performed with anti-FLAG M2 affinity gel resin (Sigma-Aldrich), and the isolated protein was analysed by immunoblotting with anti-FLAG antibodies to detect AnnAt1, AnnAt4, or GFP, and anti-HA antibodies to detect MiMIF-2. GFP, green fluorescent protein. Three independent experiments were performed with similar results. (This figure is available in color at *JXB* online.)

levels of *AnnAt1* and *AnnAt4* expression via overexpression and knockout approaches in Arabidopsis. Homozygous T3 lines overexpressing *AnnAt1* and *AnnAt4* under the control of the Super promoter (Supplementary Fig. S6C) were less susceptible to *M. incognita* than control plants (Fig. 8A), illustrated by a reduced number of galls and nematodes inside roots. In contrast, T-DNA insertional alleles of *annAt1* (*Salk_015426*) or *annAt4* (*Salk_096465*) resulted in the opposite phenotype, a higher number of galls and nematodes (Fig. 8B; Supplementary Fig. S11). These results showed the importance of annexin 1 and annexin 4 for restricting *M. incognita* infection.

The increase in $[Ca^{2+}]_{cyt}$ triggered by H_2O_2 is impaired in MiMIF-2*-expressing Arabidopsis*

Annexin 1 and annexin 4 have been shown to be involved in Ca^{2+} signature in Arabidopsis roots (Richards *et al.*, 2014; Ma *et al.*, 2019). To identify the roles of *MiMIF-2* in Ca^{2+} influx, *MiMIF-2*-OE-T3 Arabidopsis and two mutants of AnnAt1 and AnnAt4 with a reporter gene encoding *aequorin* (Supplementary Fig. S12) were challenged with H_2O_2. A transient increase in $[Ca^{2+}]_{cyt}$ was observed in all genotypes (WT, *MiMIF-2*-OE-T3, *annAt1*, and *annAt4*). However, there was a significant ($P<0.05$) difference between the maximum $[Ca^{2+}]_{cyt}$ in *aequorin*-WT (0.819±0.033 μM) *versus aequorin-MiMIF-2* (*aequorin-MiMIF-2*-OE-3: 0.579±0.055 μM; *aequorin-MiMIF-2*-OE-4: 0.592±0.011 μM), *aequorin-annAt1* (0.568±0.013 μM), and *aequorin-annAt4* (0.558±0.015 μM) (mean ±SEM; Fig. 9). Together, these results highlight the key role of *MiMIF-2* in modulating plant immune responses and Ca^{2+} signal transduction.

Discussion

MIFs have been shown to be an important endocrine immune factor in animals (Twu *et al.*, 2014; Sparkes *et al.*, 2017), and some animal parasites, including nematodes, ticks and protozoa,

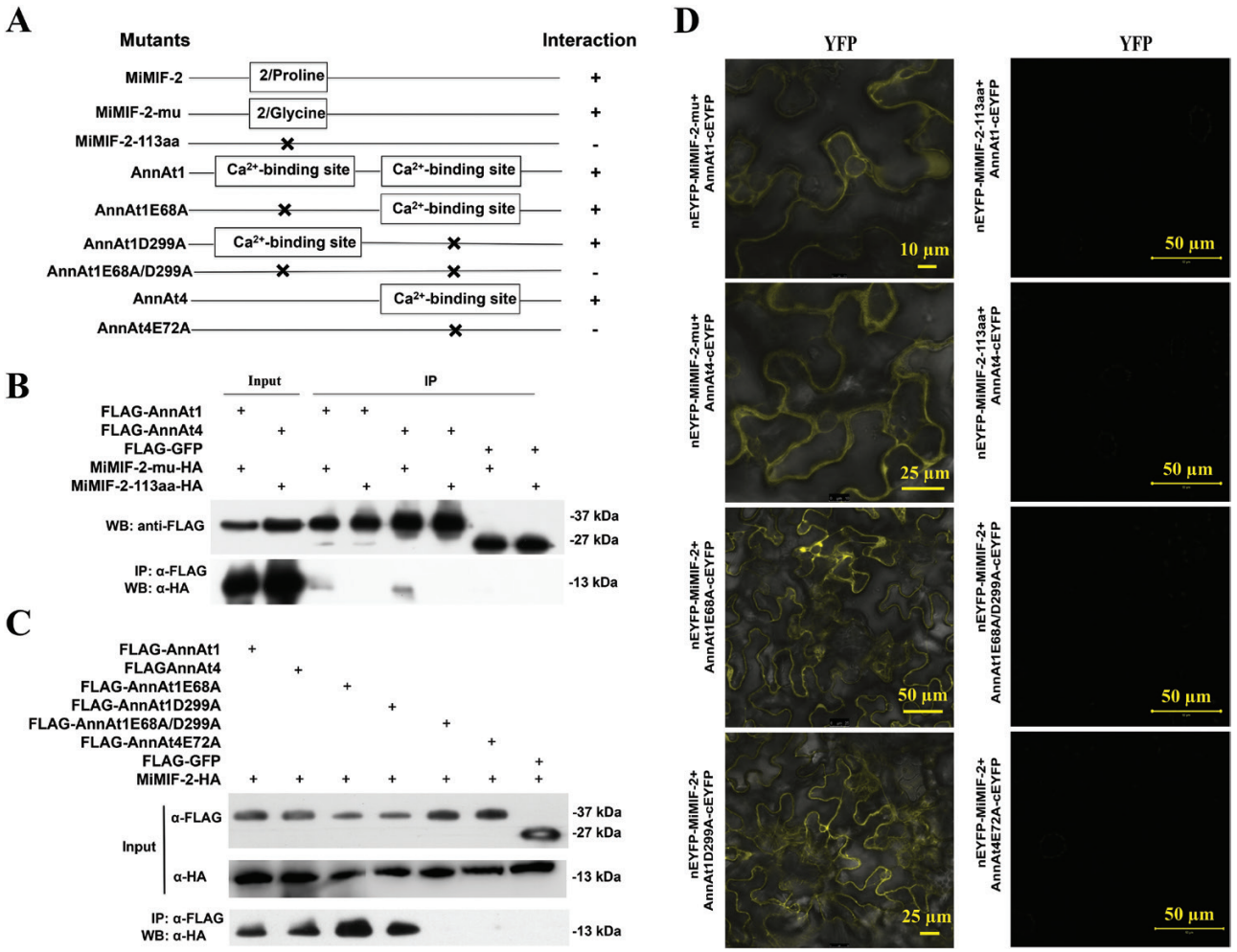

Fig. 7. The first proline residue of MiMIF-2 and the Ca^{2+}-binding sites of annexins were required for protein interaction. (A) Schematic representation of the intact, mutated, and truncated MiMIF-2 and annexin sequences used for interaction assays in tobacco leaves. The assays were performed three times, with identical results in each case. Symbols: –, no interaction; +, interaction. (B) Co-immunoprecipitation of mutated and truncated MiMIF-2 with annexins. (C) Co-immunoprecipitation of mutated annexins with MiMIF-2. (D) BiFC visualization of the mutated and truncated MiMIF-2–annexin interaction. The corresponding proteins were co-expressed in tobacco leaves. Images were taken 36 h after co-expression. Bars, 10, 25 or 50 μm as shown. GFP, green fluorescent protein; YFP, yellow fluorescent protein. All experiments were repeated three times with similar results. (This figure is available in color at *JXB* online.)

have been reported to secrete MIFs as a mechanism of host immune system evasion (Pastrana *et al.*, 1998; Falcone *et al.*, 2001). Nevertheless, only a few studies have investigated the role of MIFs in plant parasites. Aphid MIFs were secreted from *Myzus percicae* saliva and were crucial for aphid survival, fecundity, and feeding on a host plant. The ectopic expression of aphid MIFs in leaf tissues inhibits the major plant immune response (Dubreuil *et al.*, 2014; Naessens *et al.*, 2015). Interestingly, MIFs have been identified in many plant-parasitic nematodes, including cyst nematodes and RKNs (Vermeire *et al.*, 2008). We characterized MIF-like proteins of *M. incognita*, and explored their functions in plant–nematode interaction.

Secreted effectors play essential roles in nematode–host interactions. Research efforts in recent decades have focused largely on effectors from the esophageal gland cells of plant-parasitic nematodes (Hussey, 1989; Davis *et al.*, 2008; Hewezi, 2015), and there have been a few reports relating to effectors secreted onto the parasite surface. The majority of known plant nematode effectors are synthesized in specialized secretory cells, the esophageal/salivary glands. So far only a few RKN effectors have been localized inside giant cells, all in nuclei (Favery *et al.*, 2016; Chen *et al.*, 2017). *In planta* immunocytological analyses showed that the giant cell apoplasm is an important compartment of nematode stylet-secreted proteins among which are proteins that are predicted to act intracellularly such as a calreticulin (Vieira *et al.*, 2011). No mechanism of nematode effector translocation has been described and the minute amount of secreted products might prevent their detection in hypertrophied RKN-induced giant cell cytoplasm. Here we demonstrated that MiMIF-2 secreted from the hypodermis into the plant apoplast finally targets the giant cell cytoplasm (Fig. 2). This result highlights a process by which an apoplastic effector enters into plant cells.

In mammals, MIF has been shown to mediate its biological effects via two signaling mechanisms: the classical receptor-mediated pathway and a non-classical endocytic pathway (Donn and Ray, 2004). The first human MIF receptor to be identified was a cell surface class II major histocompatibility

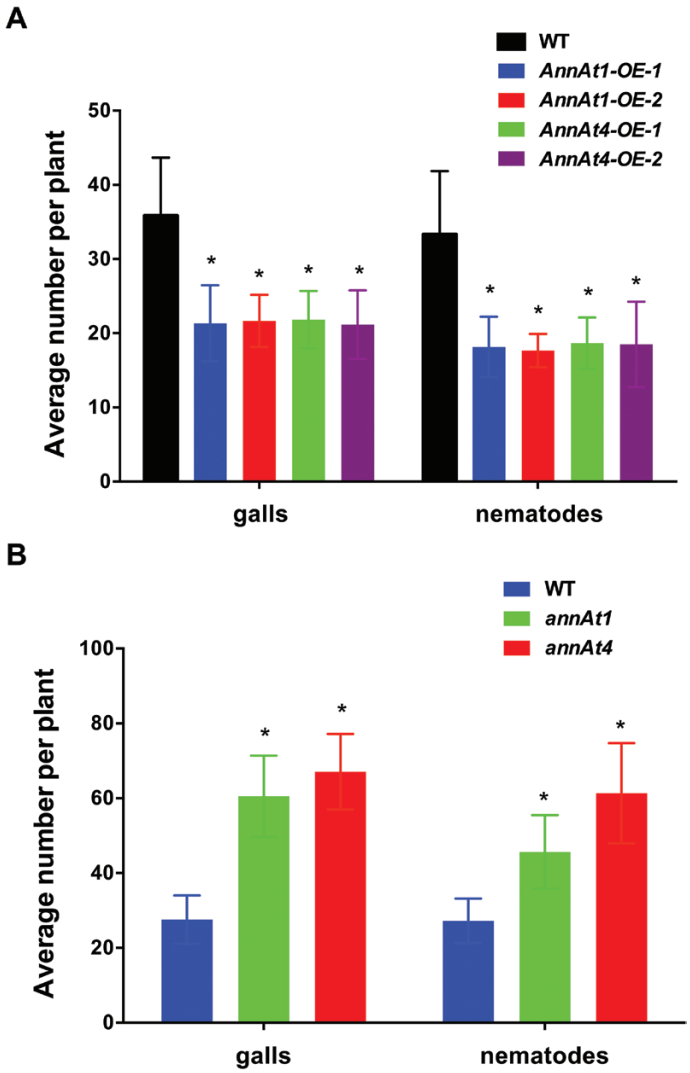

Fig. 8. AnnAt1 and AnnAt4 are involved in Arabidopsis response to *Meloidogyne incognita*. (A) Overexpression of *AnnAt1* or *AnnAt4* in Arabidopsis decreased susceptibility to *M. incognita*, as indicated by the mean numbers of galls and nematodes at 35 dpi in plant roots. (B) The two annexin mutant lines were more susceptible to *M. incognita*, as indicated by the mean numbers of nematodes and galls in plant roots. Error bars represent the mean ±SD ($n \geq 30$), and asterisks denote significant differences (*$P<0.05$, one-way ANOVA). All experiments were repeated three times with similar results, and each line counted at least 30 plants. (This figure is available in color at *JXB* online.)

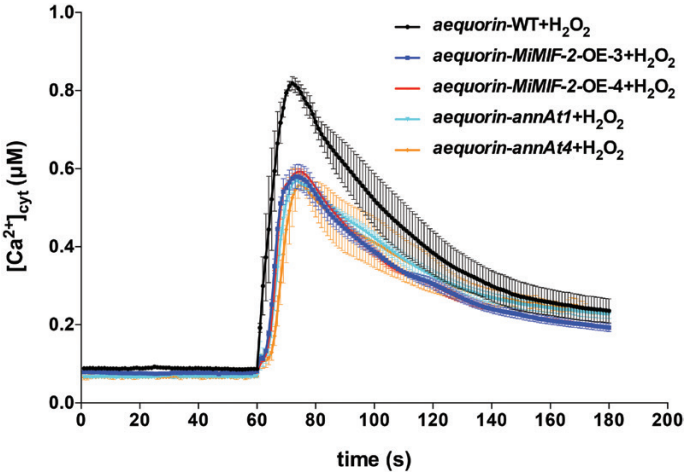

Fig. 9. The H_2O_2-induced increase in $[Ca^{2+}]_{cyt}$ is impaired in *MiMIF-2* ectopically expressing Arabidopsis lines, *annAt1* mutant line, and *annAt4* mutant line. An *aequorin* gene was expressed in 10-day-old seedlings of WT, *MiMIF-2* ectopically expressing Arabidopsis (*aequorin-MiMIF-2*-OE-3 and *aequorin-MiMIF-2*-OE-4), *annAt1* mutant line, and *annAt4* mutant line. Root $[Ca^{2+}]_{cyt}$ was assessed by measuring cytosolic aequorin concentration in response to 20 mM H_2O_2 treatment. The control response (buffer only, at 0–60 s) was similar in *aequorin*-WT, *aequorin-MiMIF-2-OE-3*, *aequorin-MiMIF-2-OE-4*, *aequorin-annAt1*, and *aequorin-annAt4*. H_2O_2 stimulation was initiated at 60 s. The data shown are mean values ±SEM (n=12). The experiments were performed three times, with similar results in each case. (This figure is available in color at *JXB* online.)

chaperone, CD74 (Leng *et al.*, 2003). MIF has also been shown to be directly taken up into target cells and to interact with intracellular signaling molecules, including the human Jun activation domain-binding protein JAB-1 (Kleemann *et al.*, 2000). The characterization of the pathway(s) used by MiMIFs, and/or endogenous plant MDLs, to enter into the plant cells would represent a breakthrough in our knowledge of the mode of action of small proteins in plants.

Host-derived RNAi silencing or ectopic expression of *MiMIFs in planta* significantly decreased or increased, respectively, the infectiousness of *M. incognita*, indicating *MiMIFs* are important for nematode parasitism (Fig. 3). Nematodes feed on viable host cells for nutrition via the stylet; thus, efficient mechanisms must be employed to suppress or evade host defenses at this stage. To achieve this, RKNs deliver several effectors into host cells to suppress immune responses including PCD (Niu *et al.*, 2016; Chen *et al.*, 2017; Naalden *et al.*, 2018; Nguyen *et al.*, 2018; Shi *et al.*, 2018). We showed that transient expression of MiMIF-2 could suppress PCD triggered by BAX or RBP1/Gpa2 (Fig. 4). In addition, the use of flg22 to stimulate the defense responses of Arabidopsis (Gómez-Gómez and Boller, 2000; Asai *et al.*, 2002; Navarro *et al.*, 2004; Lee and Back, 2016) revealed low levels of MPK3 and MPK6 phosphorylation, suppression of defense marker gene expression and low levels of callose deposition in *MiMIF-2*-expressing lines (Fig. 5). MPK3 and MPK6 are crucial positive regulators of plant defense responses; they are involved in the biosynthesis of both ethylene (Meng and Zhang, 2013) and jasmonate (Schweighofer and Meskiene, 2008). MAPK signaling in Arabidopsis roots has also been demonstrated to be activate following infection by the cyst nematode *Heterodera schachtii* (Sidonskaya *et al.*, 2016). Thus, *MiMIF-2* expression may interfere with host signal transduction and immune responses as described in mammalian cells.

In an attempt to understand how *MiMIFs* interfere with these plant pathways, we used IP-LC-MS to identify proteins that interact with MiMIF-2. BiFC and Co-IP demonstrated two annexins were targeted by MiMIF-2 in Arabidopsis (Fig. 6). MiMIF-2–AnnAt1 and MiMIF-2–AnnAt4 complexes were found to localize within the cytosol. Previous studies have indicated that AnnAt1 not only rescues a mutant *E. coli* strain lacking *OxyR* from H_2O_2 stress (Gidrol *et al.*, 1996), but also may protect (i) human tumor cells against tumor necrosis factor and (ii) mammalian cells against oxidative stress (Jänicke *et al.*, 1998; Kush and Sabapathy, 2001). AnnAt1 levels

have been shown to increase significantly during osmotic stress and powdery mildew infection (Lee *et al.*, 2004; Cantero *et al.*, 2006; Chandran *et al.*, 2010). The annexin from *Brassica juncea* (AnnBj1) gave resistance to numerous abiotic and biotic stresses in tobacco (Jami *et al.*, 2008). There is also evidence to suggest that annexins are involved in plant wound responses through their role in membrane repair (Schapire *et al.*, 2009; Clark *et al.*, 2012). Interestingly, cyst nematodes induce expression of *ANNEXIN* genes in Arabidopsis (Puthoff *et al.*, 2003) and soybean roots (Klink *et al.*, 2007) and secrete annexin-like effectors to interfere with plant immune responses. Hs4F01 could complement the function of Arabidopsis annexin 1, indicating a mimicry of plant annexins by nematode annexin. Moreover, Hs4F01 may modulate defense responses through interacting with the 2OG–Fe(II) oxygenase (DMR6) (Patel *et al.*, 2010). These results suggest dual roles of Hs4F01 during cyst nematode parasitism. However, previous studies on transcript changes of RKN-induced galls showed that the expression of Arabidopsis annexin 1 and annexin 4 were both repressed (Jammes *et al.*, 2005; Barcala *et al.*, 2010). Here, we showed that *AnnAt1*- or *AnnAt4*-overexpressing lines are more resistant to *M. incognita* and that, on the contrary, the *AnnAt1* or *AnnAt4* knockout lines are more sensitive (Fig. 8). This is in accordance with the role of annexins in plant defense. While no annexins have been shown to be secreted by root-knot nematodes, we can propose that MiMIF-2 is involved in protection of nematodes from oxidative stress by fine-tuning the plant annexin function.

Annexins are Ca^{2+}- and phospholipid-binding proteins widespread throughout the animal and plant kingdoms (Gerke and Moss, 2002; Laohavisit and Davies, 2011). Ca^{2+} is widely seen as a common and simple messenger that acts by coupling extracellular signals to cellular responses and integrating biotic and abiotic information (Dodd *et al.*, 2010; Newton *et al.*, 2016; Ranty *et al.*, 2016). Moreover, the Ca^{2+} signals act in synergy with ROS and activate MAPK cascades (Gilroy *et al.*, 2014; Lee and Back, 2016). Annexins regulate abiotic stress-induced calcium signal transduction and mediate biotic stress responses to environmental stimuli (Gorecka *et al.*, 2007; Vandeputte *et al.*, 2007; Davies, 2014; Yang *et al.*, 2014). Calcium signatures also activate various plant enzymes, even altering gene expression, and can, ultimately, modify cells and the calcium signals corresponding to their physiological and biochemical reactions (Tuteja and Mahajan, 2007; Kim *et al.*, 2009). Peroxide-induced increases in $[Ca^{2+}]_{cyt}$ were recently reported to be aberrant in roots and root epidermal protoplasts from an *annAt1*-knockout mutant, indicating an essential role for AnnAt1 in the $[Ca^{2+}]_{cyt}$ signature and downstream signaling (Richards *et al.*, 2014). Moreover, AnnAt1 interacts with AnnAt4, which is modulated by Ca^{2+} binding (Huh *et al.*, 2010), and recent studies confirmed AnnAt4 interacted with the calcium sensor SCaBP8, which regulated calcium transients and signatures in Arabidopsis (Ma *et al.*, 2019). These results inspire the possibility that plant annexins with other proteins may form complexes modulating calcium signaling. It's possible that MiMIF-2 is involved in the complexes that fine-tune annexin-mediated signal transduction and immune responses. Evidence showed that in rat testicular peritubular cells, MIF signal transduction was based on mobilizing intracellular calcium (Wennemuth *et al.*, 2000). In human neutrophils, MIF induced calcium influx by acting on two chemokine receptors, CXCR2 and CXCR4 (Bernhagen *et al.*, 2007). Here, we found that the Ca^{2+} binding sites of annexins were required for interaction between MiMIF-2 and annexins (Fig. 7). This led us to hypothesize that Ca^{2+} signal transduction might be impaired in *MiMIF-2* ectopically expressing Arabidopsis plants. Consistent with this hypothesis, Arabidopsis expressing *MiMIF-2* displayed smaller increases in $[Ca^{2+}]_{cyt}$ following stimulation with H_2O_2, i.e. a decrease Ca^{2+} influx (Fig. 9), as previously observed in *annAt1* and *annAt4* mutants (Richards *et al.*, 2014; Ma *et al.*, 2019). Our findings suggest a new model for Ca^{2+}, annexins, and pathogen effectors: the combination of annexins with effectors modulates calcium signaling, interfering with the immune response. Ultimately, our discovery further improves our understanding of effector proteins in *M. incognita* and identifies new avenues of exploration for studies investigating mechanism by which MIF-like proteins function.

Supplementary data

Supplementary data are available at *JXB* online.

Fig. S1. Characteristics of MiMIF sequences.

Fig. S2. Western blot analysis detected specificity of MiMIF-2 antibody.

Fig. S3. Ultrastructural immunocytochemistry of *M. incognita* MIF proteins.

Fig. S4. Localization of MiMIF proteins in tomato gall sections.

Fig. S5. Phenotypes of *MiMIF-2* ectopically expressing Arabidopsis and *Mimif-2-RNAi* lines.

Fig. S6. Verification, by RT-PCR and/or western blotting, of the presence of *MiMIF-2* transcripts, MiMIF-2 protein, and annexin proteins in transgenic Arabidopsis.

Fig. S7. MiMIF 2 could not interact with a chloroplasts chaperonin (AT3G13470), heat shock protein 70 (AT5G02490) and heat shock protein 9 (AT5G56010).

Fig. S8. MiMIF-2 could not interact with AnnAt2, AnnAt3, AnnAt5, and AnnAt8.

Fig. S9. Subcellular localization of AnnAt1, AnnAt4, AnnAt1E68A, AnnAt1D299A, AnnAt1E68A/D299A, and AnnAt4E72A.

Fig. S10. Subcellular localization of MiMIF-2, MiMIF-2-mu, and MiMIF-2-113aa.

Fig. S11. Verification of homozygous T-DNA insertion mutants of *annAt1* and *annAt4*.

Fig. S12. RT-PCR verification of gene expression in transgenic Arabidopsis.

Table S1. Primers used in this study.

Table S2. Accession numbers of genes or proteins used in this study.

Table S3. Candidate proteins that interact with MiMIF-2 identified by LC-MS.

Acknowledgements

The authors thank Professors Zejian Guo, Wenxian Sun, and Yan Guo (China Agricultural University, China), Yuanchao Wang (Nanjing

Agricultural University, China), and Wenqiang Tang (Hebei Normal University, China) for valuable suggestions and for providing 35S:*aequorin-annAt1/-annAt4* and *aequorin*-expressing transgenic Arabidopsis seeds, and the pGR107 vectors, respectively. We are grateful to Dr Janice de Almeida Engler for help with immunostaining, and to Drs Etienne G. J. Danchin, and Laetitia Perfus-Barbeoch (Institut Sophia Agrobiotech, ISA, France) for analysing the Illumina transcriptome data generated in the ANR program ASEXEVOL, respectively. Immunolocalization were performed at the SPIBOC imaging facility of the Institut Sophia Agrobiotech (France). This research supported by the National Key Research and Development Program of China (No. 2017YFD0200601) and the National Basic Research Program of China (No. 2013CB127501), and the National Natural Science Foundation of China (Nos. 31571987, 31772138). PA and BF were funded by INRA and the French Government (National Research Agency, ANR) through the 'Investments for the Future' LabEx SIGNALIFE: program reference no. ANR-11-LABX-0028-01. JLZ was funded by China Scholarship Council (No. 201606350083) for studying in INRA, France.

References

Abad P, Gouzy J, Aury JM, *et al*. 2008. Genome sequence of the metazoan plant-parasitic nematode *Meloidogyne incognita*. Nature Biotechnology **26**, 909–915.

Ajonina-Ekoti I, Kurosinski MA, Younis AE, *et al*. 2013. Comparative analysis of macrophage migration inhibitory factors (MIFs) from the parasitic nematode *Onchocerca volvulus* and the free-living nematode *Caenorhabditis elegans*. Parasitology Research **112**, 3335–3346.

Asai T, Tena G, Plotnikova J, Willmann MR, Chiu WL, Gomez-Gomez L, Boller T, Ausubel FM, Sheen J. 2002. MAP kinase signalling cascade in *Arabidopsis* innate immunity. Nature **415**, 977–983.

Barcala M, García A, Cabrera J, Casson S, Lindsey K, Favery B, García-Casado G, Solano R, Fenoll C, Escobar C. 2010. Early transcriptomic events in microdissected Arabidopsis nematode-induced giant cells. The Plant Journal **61**, 698–712.

Bernhagen J, Calandra T, Mitchell RA, Martin SB, Tracey KJ, Voelter W, Manogue KR, Cerami A, Bucala R. 1993. MIF is a pituitary-derived cytokine that potentiates lethal endotoxaemia. Nature **365**, 756–759.

Bernhagen J, Krohn R, Lue H, *et al*. 2007. MIF is a noncognate ligand of CXC chemokine receptors in inflammatory and atherogenic cell recruitment. Nature Medicine **13**, 587–596.

Blanc-Mathieu R, Perfus-Barbeoch L, Aury JM, *et al*. 2017. Hybridization and polyploidy enable genomic plasticity without sex in the most devastating plant-parasitic nematodes. PLoS Genetics **13**, e1006777.

Bybd DW, Kirkpatrick T, Barker KR. 1983. An improved technique for clearing and staining plant tissues for detection of nematodes. Journal of Nematology **15**, 142–143.

Caillaud MC, Dubreuil G, Quentin M, Perfus-Barbeoch L, Lecomte P, de Almeida Engler J, Abad P, Rosso MN, Favery B. 2008. Root-knot nematodes manipulate plant cell functions during a compatible interaction. Journal of Plant Physiology **165**, 104–113.

Calandra T, Roger T. 2003. Macrophage migration inhibitory factor: a regulator of innate immunity. Nature Reviews Immunology **3**, 791–800.

Cantero A, Barthakur S, Bushart TJ, Chou S, Morgan RO, Fernandez MP, Clark GB, Roux SJ. 2006. Expression profiling of the *Arabidopsis annexin* gene family during germination, de-etiolation and abiotic stress. Plant Physiology and Biochemistry **44**, 13–24.

Chandran D, Inada N, Hather G, Kleindt CK, Wildermuth MC. 2010. Laser microdissection of *Arabidopsis* cells at the powdery mildew infection site reveals site-specific processes and regulators. Proceedings of the National Academy of Sciences, USA **107**, 460–465.

Chen C, Liu S, Liu Q, Niu J, Liu P, Zhao J, Jian H. 2015. An ANNEXIN-like protein from the cereal cyst nematode *Heterodera avenae* suppresses plant defense. PLoS One **10**, e0122256.

Chen J, Lin B, Huang Q, Hu L, Zhuo K, Liao J. 2017. A novel *Meloidogyne graminicola* effector, MgGPP, is secreted into host cells and undergoes glycosylation in concert with proteolysis to suppress plant defenses and promote parasitism. PLoS Pathogens **13**, e1006301.

Cho Y, Jones BF, Vermeire JJ, *et al*. 2007. Structural and functional characterization of a secreted hookworm macrophage migration inhibitory factor (MIF) that interacts with the human MIF receptor CD74. Journal of Biological Chemistry **282**, 23447–23456.

Clark G, Konopka-Postupolska D, Hennig J, Roux S. 2010. Is annexin 1 a multifunctional protein during stress responses? Plant Signaling & Behavior **5**, 303–307.

Clark GB, Morgan RO, Fernandez MP, Roux SJ. 2012. Evolutionary adaptation of plant annexins has diversified their molecular structures, interactions and functional roles. New Phytologist **196**, 695–712.

Clark GB, Sessions A, Eastburn DJ, Roux SJ. 2001. Differential expression of members of the annexin multigene family in Arabidopsis. Plant Physiology **126**, 1072–1084.

Dafny-Yelin M, Chung SM, Frankman EL, Tzfira T. 2007. pSAT RNA interference vectors: a modular series for multiple gene down-regulation in plants. Plant Physiology **145**, 1272–1281.

Dangl JL, Horvath DM, Staskawicz BJ. 2013. Pivoting the plant immune system from dissection to deployment. Science **341**, 746–751.

David JR. 1966. Delayed hypersensitivity in vitro: its mediation by cell-free substances formed by lymphoid cell-antigen interaction. Proceedings of the National Academy of Sciences, USA **56**, 72–77.

Davies JM. 2014. Annexin-mediated calcium signalling in plants. Plants **3**, 128–140.

Davies KG, Curtis RH. 2011. Cuticle surface coat of plant-parasitic nematodes. Annual Review of Phytopathology **49**, 135–156.

Davis EL, Hussey RS, Mitchum MG, Baum TJ. 2008. Parasitism proteins in nematode-plant interactions. Current Opinion in Plant Biology **11**, 360–366.

de Almeida Engler J, Van Poucke K, Karimi M, De Groodt R, Gheysen G, Engler G, Gheysen G. 2004. Dynamic cytoskeleton rearrangements in giant cells and syncytia of nematode-infected roots. The Plant Journal **38**, 12–26.

Dodd AN, Kudla J, Sanders D. 2010. The language of calcium signaling. Annual Review of Plant Biology **61**, 593–620.

Donn RP, Ray DW. 2004. Macrophage migration inhibitory factor: molecular, cellular and genetic aspects of a key neuroendocrine molecule. The Journal of Endocrinology **182**, 1–9.

Dubreuil G, Deleury E, Crochard D, Simon JC, Coustau C. 2014. Diversification of MIF immune regulators in aphids: link with agonistic and antagonistic interactions. BMC Genomics **15**, 762.

Dubreuil G, Deleury E, Magliano M, Jaouannet M, Abad P, Rosso MN. 2011. Peroxiredoxins from the plant parasitic root-knot nematode, *Meloidogyne incognita*, are required for successful development within the host. International Journal for Parasitology **41**, 385–396.

Ellinger D, Naumann M, Falter C, Zwikowics C, Jamrow T, Manisseri C, Somerville SC, Voigt CA. 2013. Elevated early callose deposition results in complete penetration resistance to powdery mildew in Arabidopsis. Plant Physiology **161**, 1433–1444.

Falcone FH, Loke P, Zang X, MacDonald AS, Maizels RM, Allen JE. 2001. A *Brugia malayi* homolog of macrophage migration inhibitory factor reveals an important link between macrophages and eosinophil recruitment during nematode infection. The Journal of Immunology **167**, 5348–5354.

Favery B, Quentin M, Jaubert-Possamai S, Abad P. 2016. Gall-forming root-knot nematodes hijack key plant cellular functions to induce multinucleate and hypertrophied feeding cells. Journal of Insect Physiology **84**, 60–69.

Gerke V, Moss SE. 2002. Annexins: from structure to function. Physiological Reviews **82**, 331–371.

Gidrol X, Sabelli PA, Fern YS, Kush AK. 1996. Annexin-like protein from *Arabidopsis thaliana* rescues *delta oxyR* mutant of *Escherichia coli* from H_2O_2 stress. Proceedings of the National Academy of Sciences, USA **93**, 11268–11273.

Gilroy S, Suzuki N, Miller G, Choi WG, Toyota M, Devireddy AR, Mittler R. 2014. A tidal wave of signals: calcium and ROS at the forefront of rapid systemic signaling. Trends in Plant Science **19**, 623–630.

Gómez-Gómez L, Boller T. 2000. FLS2: an LRR receptor-like kinase involved in the perception of the bacterial elicitor flagellin in *Arabidopsis*. Molecular Cell **5**, 1003–1011.

Gorecka KM, Thouverey C, Buchet R, Pikula S. 2007. Potential role of annexin AnnAt1 from *Arabidopsis thaliana* in pH-mediated cellular response to environmental stimuli. Plant & Cell Physiology **48**, 792–803.

Haegeman A, Mantelin S, Jones JT, Gheysen G. 2012. Functional roles of effectors of plant-parasitic nematodes. Gene **492**, 19–31.

Hewezi T. 2015. Cellular signaling pathways and posttranslational modifications mediated by nematode effector proteins. Plant Physiology **169**, 1018–1026.

Huh SM, Noh EK, Kim HG, Jeon BW, Bae K, Hu HC, Kwak JM, Park OK. 2010. Arabidopsis annexins AnnAt1 and AnnAt4 interact with each other and regulate drought and salt stress responses. Plant & Cell Physiology **51**, 1499–1514.

Hussey RS. 1989. Disease-inducing secretions of plant-parasitic nematodes. Annual Review of Phytopathology **27**, 123–141.

Iberkleid I, Vieira P, de Almeida Engler J, Firester K, Spiegel Y, Horowitz SB. 2013. Fatty acid-and retinol-binding protein, Mj-FAR-1 induces tomato host susceptibility to root-knot nematodes. PLoS One **8**, e64586.

Ibrahim HM, Hosseini P, Alkharouf NW, Hussein EH, Gamal El-Din Ael K, Aly MA, Matthews BF. 2011. Analysis of gene expression in soybean (*Glycine max*) roots in response to the root knot nematode *Meloidogyne incognita* using microarrays and KEGG pathways. BMC Genomics **12**, 220.

Jami SK, Clark GB, Turlapati SA, Handley C, Roux SJ, Kirti PB. 2008. Ectopic expression of an annexin from *Brassica juncea* confers tolerance to abiotic and biotic stress treatments in transgenic tobacco. Plant Physiology and Biochemistry **46**, 1019–1030.

Jammes F, Lecomte P, de Almeida-Engler J, Bitton F, Martin-Magniette ML, Renou JP, Abad P, Favery B. 2005. Genome-wide expression profiling of the host response to root-knot nematode infection in Arabidopsis. The Plant Journal **44**, 447–458.

Jänicke RU, Porter AG, Kush A. 1998. A novel *Arabidopsis thaliana* protein protects tumor cells from tumor necrosis factor-induced apoptosis. Biochimica et Biophysica Acta **1402**, 70–78.

Jaouannet M, Magliano M, Arguel MJ, Gourgues M, Evangelisti E, Abad P, Rosso MN. 2013. The root-knot nematode calreticulin Mi-CRT is a key effector in plant defense suppression. Molecular Plant-Microbe Interactions **26**, 97–105.

Jaouannet M, Perfus-Barbeoch L, Deleury E, *et al*. 2012. A root-knot nematode-secreted protein is injected into giant cells and targeted to the nuclei. New Phytologist **194**, 924–931.

Jing M, Guo B, Li H, *et al*. 2016. A *Phytophthora sojae* effector suppresses endoplasmic reticulum stress-mediated immunity by stabilizing plant Binding immunoglobulin Proteins. Nature Communications **7**, 11685.

Jones JD, Dangl JL. 2006. The plant immune system. Nature **444**, 323–329.

Jones JT, Haegeman A, Danchin EG, *et al*. 2013. Top 10 plant-parasitic nematodes in molecular plant pathology. Molecular Plant Pathology **14**, 946–961.

Jones JT, Reavy B, Smant G, Prior AE. 2004. Glutathione peroxidases of the potato cyst nematode *Globodera rostochiensis*. Gene **324**, 47–54.

Kim MC, Chung WS, Yun DJ, Cho MJ. 2009. Calcium and calmodulin-mediated regulation of gene expression in plants. Molecular Plant **2**, 13–21.

Kleemann R, Hausser A, Geiger G, *et al*. 2000. Intracellular action of the cytokine MIF to modulate AP-1 activity and the cell cycle through Jab1. Nature **408**, 211–216.

Klink VP, Overall CC, Alkharouf NW, MacDonald MH, Matthews BF. 2007. Laser capture microdissection (LCM) and comparative microarray expression analysis of syncytial cells isolated from incompatible and compatible soybean (*Glycine max*) roots infected by the soybean cyst nematode (*Heterodera glycines*). Planta **226**, 1389–1409.

Kush A, Sabapathy K. 2001. Oxy5, a novel protein from *Arabidopsis thaliana*, protects mammalian cells from oxidative stress. The International Journal of Biochemistry & Cell Biology **33**, 591–602.

Lang T, Lee JPW, Elgass K, *et al*. 2018. Macrophage migration inhibitory factor is required for NLRP3 inflammasome activation. Nature Communications **9**, 2223.

Laohavisit A, Davies JM. 2009. Multifunctional annexins. Plant Science **177**, 532–539.

Laohavisit A, Davies JM. 2011. Annexins. New Phytologist **189**, 40–53.

Laohavisit A, Mortimer JC, Demidchik V, *et al*. 2009. *Zea mays* annexins modulate cytosolic free Ca^{2+} and generate a Ca^{2+}-permeable conductance. The Plant Cell **21**, 479–493.

Laohavisit A, Shang Z, Rubio L, *et al*. 2012. *Arabidopsis* annexin1 mediates the radical-activated plasma membrane Ca^{2+}- and K^+-permeable conductance in root cells. The Plant Cell **24**, 1522–1533.

Lee HY, Back K. 2016. Mitogen-activated protein kinase pathways are required for melatonin-mediated defense responses in plants. Journal of Pineal Research **60**, 327–335.

Lee S, Lee EJ, Yang EJ, Lee JE, Park AR, Song WH, Park OK. 2004. Proteomic identification of annexins, calcium-dependent membrane binding proteins that mediate osmotic stress and abscisic acid signal transduction in *Arabidopsis*. The Plant Cell **16**, 1378–1391.

Leng L, Metz CN, Fang Y, Xu J, Donnelly S, Baugh J, Delohery T, Chen Y, Mitchell RA, Bucala R. 2003. MIF signal transduction initiated by binding to CD74. Journal of Experimental Medicine **197**, 1467–1476.

Lin B, Zhuo K, Wu P, Cui R, Zhang LH, Liao J. 2013. A novel effector protein, MJ-NULG1a, targeted to giant cell nuclei plays a role in *Meloidogyne javanica* parasitism. Molecular Plant-Microbe Interactions **26**, 55–66.

Liu L, Wang Y, Cui F, Fang A, Wang S, Wang J, Wei C, Li S, Sun W. 2017. The type III effector AvrXccB in *Xanthomonas campestris* pv. *campestris* targets putative methyltransferases and suppresses innate immunity in Arabidopsis. Molecular Plant Pathology **18**, 768–782.

Livak KJ, Schmittgen TD. 2001. Analysis of relative gene expression data using real-time quantitative PCR and the $2^{-\Delta\Delta C(T)}$ method. Methods **25**, 402–408.

Lue H, Thiele M, Franz J, Dahl E, Speckgens S, Leng L, Fingerle-Rowson G, Bucala R, Lüscher B, Bernhagen J. 2007. Macrophage migration inhibitory factor (MIF) promotes cell survival by activation of the Akt pathway and role for CSN5/JAB1 in the control of autocrine MIF activity. Oncogene **26**, 5046–5059.

Ma L, Ye J, Yang Y, *et al*. 2019. The SOS2-SCaBP8 complex generates and fine-tunes an AtANN4-dependent calcium signature under salt stress. Developmental Cell **48**, 697–709.e5.

Meng X, Zhang S. 2013. MAPK cascades in plant disease resistance signaling. Annual Review of Phytopathology **51**, 245–266.

Mitchell RA, Metz CN, Peng T, Bucala R. 1999. Sustained mitogen-activated protein kinase (MAPK) and cytoplasmic phospholipase A2 activation by macrophage migration inhibitory factor (MIF). Regulatory role in cell proliferation and glucocorticoid action. Journal of Biological Chemistry **274**, 18100–18106.

Morand EF, Leech M, Bernhagen J. 2006. MIF: a new cytokine link between rheumatoid arthritis and atherosclerosis. Nature Reviews. Drug Discovery **5**, 399–410.

Naalden D, Haegeman A, de Almeida-Engler J, Birhane Eshetu F, Bauters L, Gheysen G. 2018. The *Meloidogyne graminicola* effector Mg16820 is secreted in the apoplast and cytoplasm to suppress plant host defense responses. Molecular Plant Pathology **19**, 2416–2430.

Naessens E, Dubreuil G, Giordanengo P, Baron OL, Minet-Kebdani N, Keller H, Coustau C. 2015. A secreted MIF cytokine enables aphid feeding and represses plant immune responses. Current Biology **25**, 1898–1903.

Navarro L, Zipfel C, Rowland O, Keller I, Robatzek S, Boller T, Jones JD. 2004. The transcriptional innate immune response to flg22. Interplay and overlap with *Avr* gene-dependent defense responses and bacterial pathogenesis. Plant Physiology **135**, 1113–1128.

Newton AC, Bootman MD, Scott JD. 2016. Second messengers. Cold Spring Harbor Perspectives in Biology **8**, a005926.

Nguyen CN, Perfus-Barbeoch L, Quentin M, Zhao J, Magliano M, Marteu N, Da Rocha M, Nottet N, Abad P, Favery B. 2018. A root-knot nematode small glycine and cysteine-rich secreted effector, MiSGCR1, is involved in plant parasitism. New Phytologist **217**, 687–699.

Niu J, Liu P, Liu Q, Chen C, Guo Q, Yin J, Yang G, Jian H. 2016. Msp40 effector of root-knot nematode manipulates plant immunity to facilitate parasitism. Scientific Reports **6**, 19443.

Panstruga R, Baumgarten K, Bernhagen J. 2015. Phylogeny and evolution of plant macrophage migration inhibitory factor/D-dopachrome tautomerase-like proteins. BMC Evolutionary Biology **15**, 64.

Pastrana DV, Raghavan N, FitzGerald P, Eisinger SW, Metz C, Bucala R, Schleimer RP, Bickel C, Scott AL. 1998. Filarial nematode parasites secrete a homologue of the human cytokine macrophage migration inhibitory factor. Infection and Immunity **66**, 5955–5963.

Patel N, Hamamouch N, Li C, Hewezi T, Hussey RS, Baum TJ, Mitchum MG, Davis EL. 2010. A nematode effector protein similar to annexins in host plants. Journal of Experimental Botany **61**, 235–248.

Pieterse CM, Leon-Reyes A, Van der Ent S, Van Wees SC. 2009. Networking by small-molecule hormones in plant immunity. Nature Chemical Biology **5**, 308–316.

Puthoff DP, Nettleton D, Rodermel SR, Baum TJ. 2003. *Arabidopsis* gene expression changes during cyst nematode parasitism revealed by statistical analyses of microarray expression profiles. The Plant Journal **33**, 911–921.

Quentin M, Baurès I, Hoefle C, Caillaud MC, Allasia V, Panabières F, Abad P, Hückelhoven R, Keller H, Favery B. 2016. The Arabidopsis microtubule-associated protein MAP65-3 supports infection by filamentous biotrophic pathogens by down-regulating salicylic acid-dependent defenses. Journal of Experimental Botany **67**, 1731–1743.

Ranty B, Aldon D, Cotelle V, Galaud JP, Thuleau P, Mazars C. 2016. Calcium sensors as key hubs in plant responses to biotic and abiotic stresses. Frontiers in Plant Science **7**, 327.

Richards SL, Laohavisit A, Mortimer JC, Shabala L, Swarbreck SM, Shabala S, Davies JM. 2014. Annexin 1 regulates the H_2O_2-induced calcium signature in *Arabidopsis thaliana* roots. The Plant Journal **77**, 136–145.

Robertson L, Robertson WM, Sobczak M, Helder J, Tetaud E, Ariyanayagam MR, Ferguson MA, Fairlamb A, Jones JT. 2000. Cloning, expression and functional characterisation of a peroxiredoxin from the potato cyst nematode *Globodera rostochiensis*. Molecular and Biochemical Parasitology **111**, 41–49.

Sacco MA, Koropacka K, Grenier E, Jaubert MJ, Blanchard A, Goverse A, Smant G, Moffett P. 2009. The cyst nematode SPRYSEC protein RBP-1 elicits Gpa2- and RanGAP2-dependent plant cell death. PLoS Pathogens **5**, e1000564.

Schapire AL, Valpuesta V, Botella MA. 2009. Plasma membrane repair in plants. Trends in Plant Science **14**, 645–652.

Schweighofer A, Meskiene I. 2008. Regulation of stress hormones jasmonates and ethylene by MAPK pathways in plants. Molecular BioSystems **4**, 799–803.

Shi Q, Mao Z, Zhang X, *et al*. 2018. The novel secreted *Meloidogyne incognita* effector MilSE6 targets the host nucleus and facilitates parasitism in *Arabidopsis*. Frontiers in Plant Science **9**, 252.

Shi X, Leng L, Wang T, *et al*. 2006. CD44 is the signaling component of the macrophage migration inhibitory factor-CD74 receptor complex. Immunity **25**, 595–606.

Sidonskaya E, Schweighofer A, Shubchynskyy V, Kammerhofer N, Hofmann J, Wieczorek K, Meskiene I. 2016. Plant resistance against the parasitic nematode *Heterodera schachtii* is mediated by MPK3 and MPK6 kinases, which are controlled by the MAPK phosphatase AP2C1 in Arabidopsis. Journal of Experimental Botany **67**, 107–118.

Sparkes A, De Baetselier P, Roelants K, De Trez C, Magez S, Van Ginderachter JA, Raes G, Bucala R, Stijlemans B. 2017. The non-mammalian MIF superfamily. Immunobiology **222**, 473–482.

Teixeira MA, Wei L, Kaloshian I. 2016. Root-knot nematodes induce pattern-triggered immunity in *Arabidopsis thaliana* roots. New Phytologist **211**, 276–287.

Tripathy BC, Oelmüller R. 2012. Reactive oxygen species generation and signaling in plants. Plant Signaling & Behavior **7**, 1621–1633.

Tuteja N, Mahajan S. 2007. Calcium signaling network in plants: an overview. Plant Signaling & Behavior **2**, 79–85.

Twu O, Dessi D, Vu A, *et al*. 2014. *Trichomonas vaginalis* homolog of macrophage migration inhibitory factor induces prostate cell growth, invasiveness, and inflammatory responses. Proceedings of the National Academy of Sciences, USA **111**, 8179–8184.

Vandeputte O, Lowe YO, Burssens S, Van Raemdonck D, Hutin D, Boniver D, Geelen D, El Jaziri M, Baucher M. 2007. The tobacco *Ntann12* gene, encoding an annexin, is induced upon *Rhodoccocus fascians* infection and during leafy gall development. Molecular Plant Pathology **8**, 185–194.

Vermeire JJ, Cho Y, Lolis E, Bucala R, Cappello M. 2008. Orthologs of macrophage migration inhibitory factor from parasitic nematodes. Trends in Parasitology **24**, 355–363.

Vieira P, Danchin EG, Neveu C, *et al*. 2011. The plant apoplasm is an important recipient compartment for nematode secreted proteins. Journal of Experimental Botany **62**, 1241–1253.

Walter M, Chaban C, Schütze K, *et al*. 2004. Visualization of protein interactions in living plant cells using bimolecular fluorescence complementation. The Plant Journal **40**, 428–438.

Wennemuth G, Aumüller G, Bacher M, Meinhardt A. 2000. Macrophage migration inhibitory factor-induced Ca^{2+} response in rat testicular peritubular cells. Biology of Reproduction **62**, 1632–1639.

Xu L, Li Y, Sun H, Zhen X, Qiao C, Tian S, Hou T. 2013. Current developments of macrophage migration inhibitory factor (MIF) inhibitors. Drug Discovery Today **18**, 592–600.

Xue B, Hamamouch N, Li C, Huang G, Hussey RS, Baum TJ, Davis EL. 2013. The *8D05* parasitism gene of *Meloidogyne incognita* is required for successful infection of host roots. Phytopathology **103**, 175–181.

Yang L, Zhang J, He J, Qin Y, Hua D, Duan Y, Chen Z, Gong Z. 2014. ABA-mediated ROS in mitochondria regulate root meristem activity by controlling *PLETHORA* expression in *Arabidopsis*. PLoS Genetics **10**, e1004791.

Zhang X, Henriques R, Lin SS, Niu QW, Chua NH. 2006. *Agrobacterium*-mediated transformation of *Arabidopsis thaliana* using the floral dip method. Nature Protocols **1**, 641–646.